Two neuronal peptides encoded from a single transcript regulate mitochondrial function in *Drosophila*

Justin A. Bosch[1,*], Berrak Ugur[2,†], Israel Pichardo-Casas[1], Jorden Rabasco[1], Felipe Escobedo[1], Zhongyuan Zuo[2], Ben Brown[3], Susan Celniker[3], David Sinclair[1], Hugo Bellen[2,4-6], and Norbert Perrimon[1,6,*].

1) Department of Genetics, Blavatnick Institute, Harvard Medical School, Boston, MA.
2) Department of Molecular and Human Genetics, BCM, Houston, TX 77030, USA
3) Lawrence Berkeley National Laboratory, Berkeley, CA.
4) Jan and Dan Duncan Neurological Research Institute, Texas Children's Hospital, Houston, TX 77030, USA
5) Department of Neuroscience, BCM, Houston, TX 77030, USA
6) Howard Hughes Medical Institute

[†]Current address: Departments of Neuroscience and Cell Biology, Howard Hughes Medical Institute, Yale University School of Medicine, New Haven, Connecticut 06510, USA

***Corresponding authors:**

Justin A. Bosch and Norbert Perrimon (lead contact)
Harvard Medical School
77 Avenue Louis Pasteur
Dept. of Genetics, NRB 336
Boston, MA 02115
617-432-7672
Email: perrimon@genetics.med.harvard.edu (lead contact)
jabosch@hms.harvard.edu

Summary:

Naturally produced peptides (<100 amino acids) are important regulators of physiology, development, and metabolism. Recent studies have predicted that thousands of peptides may be translated from transcripts containing small open reading frames (smORFs). Here, we describe two previously uncharacterized peptides in *Drosophila* encoded by conserved smORFs, Sloth1 and Sloth2. These peptides are translated from the same bicistronic transcript and share sequence similarities, suggesting that they encode paralogs. We provide evidence that Sloth1/2 are highly expressed in neurons, localize to mitochondria, and form a complex. Double mutant analysis in animals and cell culture revealed that *sloth1* and *sloth2* are not functionally redundant, and their loss causes animal lethality, reduced neuronal function, impaired mitochondrial function, and neurodegeneration. These results suggest that phenotypic analysis of smORF genes in *Drosophila* can provide a wealth of information on the biological functions of this poorly characterized class of genes.

Keywords: smORF, peptide, paralogs, mitochondria, bicistronic transcript, neurodegeneration, *Drosophila*, CRISPR/Cas9

Introduction

Naturally produced peptides are regulators of metabolism, development, and physiology. Well-known examples include secreted peptides that act as hormones (Pearson *et al.* 1993), signaling ligands (Katsir *et al.* 2011), or neurotransmitters (Snyder and Innis 1979). This set of peptides are produced by cleavage of larger precursor proteins (Fricker 2005), peptides can also be directly translated from a transcript with a small open reading frame (smORF) (Couso and Patraquim 2017; Plaza *et al.* 2017; Hsu and Benfey 2018; Yeasmin *et al.* 2018). Due to their small size (<100 codons), smORFs have been understudied. For example, smORFs are under represented in genome annotations (Basrai *et al.* 1997), are theoretically a poor target for EMS mutagenesis, and are often ignored in proteomic screens. Consequently, there is growing interest in this class of protein-coding gene as a potentially rich source of novel bioactive peptides.

A major obstacle in identifying smORFs that encode functionally important peptides is distinguishing them from the enormous number of smORFs present in the genome by chance (e.g. 260,000 in yeast) (Basrai *et al.* 1997). Many groups have identified and categorized smORFs with coding potential using signatures of evolutionary conservation, ribosomal profiling, and mass spectrometry (Saghatelian and Couso 2015; Couso and Patraquim 2017; Plaza *et al.* 2017). Together, these approaches suggest there may be hundreds, possibly thousands, of unannotated smORF genes. However, these “omics” methods do not tell us which smORFs encode peptides with important biological functions.

Functional characterization of smORF genes in cell lines and model organisms has the potential to confidently identify novel peptides. Historically, unbiased genetic screens and gene cloning led to the fortuitous identification and characterization of smORF peptides (e.g. POLARIS (Casson *et al.* 2002), RpL41 (Suzuki *et al.* 1990), Nedd4 (Kumar *et al.* 1993), *Drosophila* pri/tal (Galindo *et al.* 2007)). More recently, candidate bioinformatically-predicted smORF-encoded peptides (aka SEPs) have been targeted for characterization (e.g., DWORF (Nelson *et al.* 2016), Elabela/toddler (Chng *et al.* 2013; Pauli *et al.* 2014), Myomixer (Bi *et al.* 2017), Myoregulin (Anderson *et al.* 2015), and Sarcolamban (Magny *et al.* 2013), and Hemotin (Pueyo *et al.* 2016)). Collectively, these studies have been invaluable for assigning biological functions to smORF peptides. Therefore, continued functional characterization is needed to tackle the enormous number of predicted smORF peptides.

Here, through an effort to systematically characterize human-conserved smORF genes in *Drosophila* (in preparation), we identified two previously unstudied smORF peptides CG32736-PB and CG42308-PA that we named Sloth1 and Sloth2 based on their mutant phenotypes . Remarkably, both peptides are translated from the same transcript and share amino acid sequence similarity, suggesting that they encode paralogs. Loss of function analysis revealed that

each peptide is essential for viability, and mutant animals exhibit defective neuronal function and photoreceptor degeneration. These phenotypes can be explained by our finding that Sloth1 and Sloth2 localize to mitochondria and play an important role in respiration and ATP production. Finally, we propose that both peptides can bind in a shared complex. These studies uncover two new components of the mitochondria and demonstrate how functional characterization of smORFs will lead to novel biological insights.

Results

sloth1 and *sloth2* are translated from the same transcript and are likely distantly-related paralogs

Current gene annotations for *sloth1* and *sloth2* (aka *CG32736* and *CG42308*, respectively) indicate that they are expressed from the same transcript (Flybase, Figure 1A), known as a bicistronic (or dicistronic) gene (BLUMENTHAL 2004; CROSBY *et al.* 2015; KARGINOV *et al.* 2017). For example, nearby transcription start sites (Figure 1A) are predicted to only generate transcripts that encode both peptides (HOSKINS *et al.* 2011). In addition, a full-length transcript containing both smORFs is present in the cDNA clone RE60462 (GenBank Acc# AY113525), which was derived from an embryonic library (STAPLETON *et al.* 2002), and we detected the full-length bicistronic transcript from total RNA 3rd instar larvae by RT-PCR amplification (not shown). In addition, the encoded peptides Sloth1 and Sloth2 have subtle sequence similarity (27%), are similar in size (79aa and 61aa, respectively), and each contain a predicted single transmembrane domain (Figure 1B). While this type of gene structure is relatively rare in eukaryotes (BLUMENTHAL 2004; KARGINOV *et al.* 2017), there are known cases in *Drosophila* of multicistronic transcripts encoding smORF paralogs – the *pri/tal* locus (GALINDO *et al.* 2007) and the *Sarcolamban* locus (MAGNY *et al.* 2013). Furthermore, it is well known that paralogs are often found adjacent to each other in the genome due to tandem duplication (TAYLOR AND RAES 2004). Therefore, we propose that *sloth1* and *sloth2* are paralogs translated from the same transcript.

Sloth1 and Sloth2 closely resemble their human orthologs (SMIM4 and C12orf73), based on sequence similarity, similar size, and presence of a transmembrane domain (Figure 1B). Like Sloth1 and Sloth2, SMIM4 and C12orf73 also have subtle amino acid sequence similarity to each other (Figure 1B). In addition, *sloth1* and *sloth2* are conserved in other eukaryotic species (Figure 1C). Remarkably, *sloth1* and *sloth2* orthologs in choanoflagelate, sea squirt, and lamprey exhibit a similar gene architecture as *Drosophila* (Figure 1C, Supplemental File 1). In contrast, *sloth1* and *sloth2* orthologs in jawed vertebrates (e.g. mammals) are located on different chromosomes (e.g. human Chr.3 and Chr.12, respectively). Interestingly, we only found one ortholog similar to *sloth2* in the evolutionarily distant *Plasmodium*, and two orthologs similar to *sloth2* in *Arabidopsis*, which are located on different chromosomes (Figure 1C). Therefore, we hypothesize that the *sloth1* and *sloth2* ORFs duplicated from an

ancient single common ancestor ORF and became unlinked in animals along the lineage to jawed vertebrates.

We next investigated *sloth1* and *sloth2* translation parameters and efficiency, since their ORFs are frameshifted relative to each other (Figure 1A) and they are not separated by an obvious internal ribosome entry site (IRES) (VAN DER KELEN *et al.* 2009). Remarkably, there are only five nucleotides that separate the stop codon of the upstream ORF (*sloth1*) and the start codon of the downstream ORF (*sloth2*) (Figure 1A). Therefore, *sloth1* should be translated first and inhibit translation of *sloth2*, similar to the functions of so-called upstream ORFs (uORFs) (THOMPSON 2012). However, *sloth1* has a non-optimal Kozak sequence 5' to the start codon (*ACACATG*) and *sloth2* has an optimal Kozak (*CAAAATG*) (CAVENER 1987). Therefore, scanning ribosomes may occasionally fail to initiate translation on *sloth1*, in which case they would continue scanning and initiate translation on *sloth2*, known as a "leaky scanning" translation mechanism (THOMPSON 2012).

To test this translation model, we constructed an expression plasmid with the *Renilla Luciferase* (*RLuc*) reporter gene downstream of *sloth1* (*sloth1-RLuc*), while retaining non-coding elements of the original transcript (5' UTR, Kozak sequences, 5bp intervening sequence) (Figure 1D). By transfecting this reporter plasmid into *Drosophila* S2R+ cells, along with a *Firefly Luciferase* (*FLuc*) control plasmid, we could monitor changes in translation of the downstream ORF by the ratio of RLuc/FLuc luminescence. Using derivatives of the reporter plasmid with Kozak or ATG mutations, we found that translation of the downstream ORF increased when translation of *sloth1* was impaired (Figure 1E). Reciprocally, translation of the downstream ORF was decreased when *sloth1* translation was enhanced with an optimal Kozak. These results suggest that *sloth1* inhibits translation of *sloth2*, and that balanced translation of both smORFs from the same transcript might be achieved by suboptimal translation of *sloth1*.

***sloth1* and *sloth2* are essential in *Drosophila* with non-redundant function**

To determine if *sloth1* and *sloth2* have important functions in *Drosophila*, we used in vivo loss of function genetic tools. We used RNA interference (RNAi) to knock down the *sloth1-sloth2* bicistronic transcript. Ubiquitous expression of an shRNA targeting the *sloth1* coding sequence (Figure 2A) lead to significant knockdown of the *sloth1-sloth2* transcript in 3rd instar larvae (Figure 2B), as determined by two different primer pairs that bind to either the *sloth1* or *sloth2* coding sequence. Ubiquitous RNAi knockdown of *sloth1-sloth2* throughout development lead to reduced number of adult flies compared to a control (Figure 2C). This reduced viability was largely due to adult flies sticking in the food after they eclosed from their pupal cases (Figure 2D). The occasional escaper knockdown flies were slow-moving and showed only 30% climbing ability compared to control flies (Figure 2E). RNAi knockdown flies also had short scutellar bristles (Figure 2F).

We confirmed our RNAi results using CRISPR/Cas9 to generate somatic knockout (KO) flies. By crossing flies ubiquitously expressing Cas9 (*Act-Cas9)* with flies expressing an sgRNA that targets the coding sequence of either *sloth1* or *sloth2* (Figure 2A, Supplemental Figure 1A), the resulting progeny will be mosaic for insertions and deletions (indels) that cause loss of function in somatic cells (PORT *et al.* 2014; XUE *et al.* 2014). Both *sloth1* and *sloth2* somatic KO flies had significantly reduced viability compared to control (Figure 2G). Furthermore, most escaper adults had short scutellar bristles (Figure 2H) and frequently appeared sluggish (not shown). Importantly, similar phenotypes were observed when targeting either *sloth1* or *sloth2*.

Next, we further confirmed our loss of function results using CRISPR/Cas9 in the germ line to generate KO lines for *sloth1* and *sloth2*. These reagents are particularly important to test if *sloth1* and *sloth2* have redundant function by comparing the phenotypes of single and double null mutants. We generated four KO lines (Figure 2A, Supplemental Figure 1A-C): 1) a frameshift indel in *sloth1* (*sloth1*-KO), 2) a frameshift indel in *sloth2* (*sloth2*-KO), 3) a 552 bp deletion of the *sloth1* and *sloth2* reading frames (dKO), and 4) a knock-in of the reporter gene *Gal4* that removes *sloth1* and *sloth2* coding sequences (*Gal4-KI*). Since *sloth1* and *sloth2* are on the X-chromosome, we analyzed mutant hemizygous male flies. All four mutant lines were hemizygous lethal, which were rescued by a genomic transgene (Figure 2I,), ruling out off-target lethal mutations on the X-chromosome. Like RNAi and somatic KO results, rare mutant adult escaper flies had slower motor activity (Figure 2J) and short scutellar bristles (Figure 2K). Furthermore, the short scutellar bristle phenotype and slower motor activity could be rescued by a genomic transgene (Figure 2J, K).

The phenotypic similarity of single and double mutants suggests that *sloth1* and *sloth2* are not functionally redundant. However, since both ORFs are encoded on the same transcript, it is unclear if mutating one ORF will affect the other. For example, a premature stop codon can induce non-sense mediated decay of an entire transcript (NICKLESS *et al.* 2017). To address this possibility, we performed additional fly lethality rescue experiments. First, transheterozygous female flies (*sloth1-KO*/+, *sloth2-KO*/+) were viable and had normal scutellar bristles (not shown). Second, we created single ORF versions of a genomic rescue transgene – {Δ*sloth1-sloth2*} and {*sloth1*-Δ*sloth2*} (Supplemental Figure 1A). We found that *sloth1-KO* lethality could only be rescued by {*sloth1*-Δ*sloth2*}, and vice versa, *sloth2-KO* lethality could only rescued by {Δ*sloth1-sloth2*} (Figure 2L). Furthermore, single ORF rescue transgenes were unable to rescue the lethality of *dKO* and *Gal4-KI* lines (Figure 2L). Third, we used the Gal4/UAS system (BRAND AND PERRIMON 1993) to rescue mutant lethality with ubiquitously expressed cDNA transgenes. These results showed that single ORF KOs could only be rescued by expression of the same ORF (Figure 2L). Similar results were found by expressing cDNAs encoding the human orthologs (Figure 2L). In all, these results show that both *sloth1* and *sloth2* are essential, have similar loss of

function phenotypes, are not functionally redundant with one another, and are likely to retain the same function as their human orthologs.

Loss of *sloth1* and *sloth2* leads to defective neuronal function and degeneration

Since loss of *sloth1* and *sloth2* caused reduced adult mobility and climbing defects (Figure 2E, J), we speculated that the two peptides normally play an important role in cell types such as muscle or neurons. To determine where *sloth1* and *sloth2* are expressed, we used the *Gal4-KI* line as an in vivo transcriptional reporter. *Gal4-KI* mobility defects and lethality could be rescued by expressing the entire bicistronic transcript (*UAS-sloth1-sloth2*) (Figure 2J, L), or coexpression of both smORFs as cDNA (*UAS-sloth1* and *UAS-sloth2)* (Figure 2L, not shown). The *Gal4-KI* line is thus an accurate reporter of *sloth1* and *sloth2* expression. By crossing *Gal4-KI* flies with a *UAS-GFP* fluorescent reporter, we observed strong GFP expression in larval (Figure 3A, B) and adult brains (Figure 3C). In addition, *Gal4-KI* is expressed in motor neurons at the larval neuromuscular junction (NMJ) (Figure 3D) and in larval brain cells that are positive for the neuronal marker Elav (Figure 3E).

We then tested if *sloth1* and *sloth2* were important for neuronal function by measuring neuronal electrical activity in *dKO* animals. Electrical recordings taken from the larval NMJ showed that *dKO* motor neurons have normal excitatory junction potential (EJP) under resting conditions at 0.75 mM Ca^{2+} (Supplemental Figure 2). However, under high frequency stimulation (10hz), *dKO* NMJs could not sustain a proper response (Figure 4A), indicating that there is a defect in maintaining synaptic vesicle pools. Importantly, this phenotype is rescued by a genomic transgene. To test if a similar defect is present in the adults, we assessed phototransduction and synaptic transmission in photoreceptors via electroretinogram (ERG) recordings (Wu and Wong 1977; Hardie and Raghu 2001). ERGs recorded from young (1-3 days old) *dKO* photoreceptors showed an amplitude similar to that of genomic rescue animals (Figure 4B). However, upon repetitive light stimulation, ERG amplitudes were significantly reduced (Figure 4B), suggesting a gradual loss of depolarization. Similar results were observed when young flies were raised in 24hr dark (Figure 4C). Moreover, ERG traces also showed a progressive loss of “on” and “off” transients (Figure 4B, C), which is indicative of decreased synaptic communication between the photoreceptor and the postsynaptic neurons. ERG phenotypes are rescued by a full-length genomic rescue transgene, but not by single ORF rescue transgenes (Figure 4B, C). To test if loss of both *sloth1* and *sloth2* lead to neurodegeneration, we aged the animals for 4-weeks in 12hr light/dark cycle or constant darkness and recorded ERGs. Similar to young animals, aged animals raised in light/dark conditions also displayed a reduction in ERG amplitude upon repetitive stimulation (Figure 4E). These results indicate that both *sloth1* and *sloth2* are required for sustained neuronal firing in larval motor neurons and adult photoreceptors. Interestingly, similar mutant phenotypes in the NMJ and

photoreceptors are known to be due to defects in ATP production (VERSTREKEN *et al.* 2005; SANDOVAL *et al.* 2014; JAISWAL *et al.* 2015).

In addition to measuring neuronal activity, we analyzed *dKO* neurons for changes in morphology and molecular markers. Confocal imaging of the NMJ in *dKO* 3rd instar larvae did not reveal obvious changes in synapse morphology or markers of synapse function (Supplemental Figure 3). In contrast, using transmission electron microscopy (TEM) of sectioned adult eyes, we observed reduced photoreceptor number and aberrant morphology such as enlarged photoreceptors and thinner glia in *dKO* animals (Figure 5A-C), suggestive of degeneration. These phenotypes were rescued by a genomic transgene, but not with single ORF rescue constructs (Figure 5A-C, Supplemental Figure 4). Furthermore, these phenotypes were similar between young and aged flies, as well as aged flies raised in the dark (Figure 5A-C, Supplemental Figure 4). It is known that mutations affecting the turnover of Rhodopsin protein (Rh1) can lead to photoreceptor degeneration (ALLOWAY *et al.* 2000; JAISWAL *et al.* 2015). To test if this mechanism is occurring in *dKO* photoreceptors, we imaged Rh1 protein levels using confocal microscopy. We observed Rh1 accumulation in degenerating *dKO* photoreceptors in 4 week aged flies exposed to light (Figure 5D). However, Rh1 accumulation was milder in 4 week aged flies raised in the dark (Supplemental Figure 5). These results point out that light stimulation, and hence activity, enhance degeneration due to Rh1 accumulation in *dKO* animals.

Sloth1 and Sloth2 localize to mitochondria

To understand the cellular functions of Sloth1 and Sloth2, determined their subcellular localization. Using 11 domain prediction programs (Figure 6A), we found that Sloth1 orthologs have a mitochondrial-targeting motif and Sloth2 orthologs have a secretion signal (Figure 6B). This difference in predicted localization was unexpected, especially considering that these peptides are likely paralogs. Therefore, we directly visualized their subcellular location. We raised antibodies to Sloth1 and Sloth2, but were unable to detect the endogenous peptides by immunostaining and western blotting (not shown). Nevertheless, by overexpressing FLAG-tagged versions of the peptides in transfected S2R+ cells, we found that both Sloth1 and Sloth2 colocalize with mitochondrial ATP5α (Figure 6C).

We used proteomics to determine if Sloth1 and Sloth2 have interacting partners. Using *Drosophila* S2R+ cells that stably expressed Sloth1 or Sloth2 fused with a streptavidin-binding peptide (SBP) on their C-terminus (YANG AND VERAKSA 2017), we enriched complexes on streptavidin beads, identified bound proteins by mass spectrometry, and proteomic hits were tested by co-immunoprecipitation (Figure 6D). We confirmed that the Translocase of the inner membrane (Tim) complex of proteins, Tim8 and Tim13, was pulled down with Sloth1 (Figure 6E-G), and to a lesser extent Tim8 was pulled down with Sloth2 (Figure 6G). Tim8 and Tim13 form a complex in the mitochondrial intermembrane space, where

they act as a chaperone to bind and stabilize transmembrane proteins that transit to the inner mitochondrial membrane (CHACINSKA *et al.* 2009). The deep learning algorithm DeepMito (SAVOJARDO *et al.* 2020) predicts that Sloth1 orthologs localize to the mitochondrial inner membrane, and its domain structure is similar to other inner membrane proteins (CHACINSKA *et al.* 2009). Therefore, our results suggest that Sloth1 and Sloth2 localize to mitochondria, likely to the inner membrane.

It is unclear why Sloth2 has a predicted secretion signal if it localizes to mitochondria. One possibility is that the N-terminus is recognized as a bone fide mitochondrial-targeting signal, but current bioinformatic software misidentifies this motif. Alternatively, Sloth2 may dually localize to mitochondria and the secretory pathway. To test this, we determined if superfolder GFP (sfGFP)-tagged Sloth1 and Sloth2 were secreted into cell culture media from transfected S2R+ cells. Interestingly, we detected both Sloth1-sfGFP and Sloth2-sfGFP in cell culture media, at higher levels than a non-secreted mitochondrial protein (Tom20), though at lower levels than two known secreted proteins (Supplemental Figure 6A, B). Deletion of the Sloth2 secretion signal, or the Sloth1 mitochondrial targeting signal, reduced the amount sfGFP-tagged protein in the media. In addition, the Sloth2 secretion signal alone was sufficient to drive secretion of sfGFP. These results suggest that Sloth1 and Sloth2 may be secreted in addition to localizing to mitochondria.

Sloth1 and Sloth2 are important for mitochondrial function

Mutations in *Drosophila* mitochondrial genes are known to cause phenotypes that are reminiscent of loss of *sloth1* and *sloth2*, such as pupal lethality, developmental delay (not shown), reduced neuronal activity, photoreceptor degeneration, and Rh1 accumulation in photoreceptors (JAISWAL *et al.* 2015). Therefore, we tested whether *sloth1* and *sloth2* were important for mitochondrial function.

A method of assaying defects in mitochondrial function is measuring cellular oxygen consumption from live cells with a Seahorse stress test. Since this typically involves assaying a monolayer of cells, we generated KO S2R+ cell lines using CRISPR/Cas9. Compared to control cells, single KO and double KO S2R+ cells (Supplemental Figure 7A, B) had reduced basal respiration (Figure 7A, B), ATP production (Supplemental Figure 7C), and proton leaks (Supplemental Figure 7D). Results were similar for single KO and dKO lines. These results suggest that both *sloth1* and *sloth2* are important for mitochondrial function in S2R+ cells.

Next, we assayed *sloth1* and *sloth2* mutant flies for defects in mitochondrial function. ATP levels are an important indicator of mitochondrial function (KANN AND KOVACS 2007; GOLPICH *et al.* 2017) and mutations in *Drosophila* mitochondrial genes can lead to reduced ATP levels (JAISWAL *et al.* 2015).

Indeed, *dKO* larvae had ~60% ATP compared to control larvae, which was rescued by a genomic transgene (Figure 7C). Impaired mitochondrial function can also lead to cellular stress responses, such as increased expression of the mitochondrial chaperone Hsp60 (PELLEGRINO *et al.* 2013). Western blot analysis showed that *Drosophila* Hsp60 was elevated in lysates from mutant larval brains compared to control, and this effect was rescued by a genomic transgene (Figure 7D). Finally, mitochondrial dysfunction can cause changes in mitochondrial morphology and number (TREVISAN *et al.* 2018). There were no obvious changes in mitochondrial morphology in mutant larval motor neurons (Supplemental Figure 3, Supplemental Figure 7E), and adult mutant photoreceptors contained mitochondria with normal cristae (Figure 7E). In contrast, mitochondrial number was increased in mutant photoreceptors in aged animals (Figure 7E, Supplemental Figure 8A) and decreased in mutant photoreceptors in young animals (Figure 7F, Supplemental Figure 8B). In all, these data suggest that Sloth1 and Sloth2 localize to mitochondria and are important to support mitochondrial function and thus ATP production.

Sloth1 and Sloth2 may act in a stoichiometric complex

Since Sloth1 and Sloth2 share the same loss of function phenotypes and subcellular localization, we speculated that Sloth1 and Sloth2 could physically interact. Indeed, some paralogs are known to bind to the same protein complex (SZKLARCZYK *et al.* 2008) and there is a tendency for proteins in the same complex to be co-expressed (PAPP *et al.* 2003). Interestingly, our mass spectrometry results showed that Sloth1 was identified from pull-downs using Sloth2-SBP as bait. To confirm this putative interaction between Sloth1 and Sloth2, we used co-immunoprecipitation and western blotting. This revealed that Sloth1-FLAG could pull down Sloth2-HA (Figure 8A), and Sloth2-FLAG (Figure 8B) or Sloth2-SBP (Figure 8C) could pull down Sloth1-HA. Unexpectedly, we noticed that the levels of tagged peptide in cell lysates were higher when the opposite peptide was overexpressed (Figure 8A-C). Proteins in a complex commonly have important stoichiometry and unbound proteins can be degraded to preserve this balance (PAPP *et al.* 2003; SOPKO *et al.* 2006; VEITIA *et al.* 2008; PRELICH 2012; BERGENDAHL *et al.* 2019). Therefore, this data suggests that Sloth1 and Sloth2 act in a complex, where they stabilize each other's protein levels.

Imbalanced protein complex stoichiometry can lead to haploinsufficient or dominant negative phenotypes (PAPP *et al.* 2003; SOPKO *et al.* 2006; VEITIA *et al.* 2008; PRELICH 2012; BERGENDAHL *et al.* 2019). For example, gene overexpression can sometimes cause phenotypes that resemble loss of function of complex members (SOPKO *et al.* 2006; PRELICH 2012). To test this, we generated stable transgenic S2R+ cell lines overexpressing *sloth1* or *sloth2* and assayed their oxygen consumption on a Seahorse instrument. Using a copper-inducible promoter, we overexpressed the cDNA for either ORF for 16hr before measuring oxygen consumption. Seahorse results showed a decrease in basal

respiration (Figure 8D,E), ATP production (Supplemental Figure 9A), and proton leak (Supplemental Figure 9B) in overexpressing cells, strikingly similar to seahorse results in KO cells (Figure 7A-B, Supplemental Figure 9C,D). Furthermore, prolonged overexpression of either ORF reduced proliferation (Figure 8F).

Finally, we tested for *sloth1* or *sloth2* overexpression phenotypes in vivo. Low-level ubiquitous overexpression (using *da-Gal4*) of either *sloth1* or *sloth2* had no effect on fly viability or bristle length (Figure 2L, not shown). To increase expression levels, we used the strong ubiquitous driver *tub-Gal4*. Whereas *tub>sloth1* flies were viable (Figure 8G) and had normal bristle length (not shown), *tub>sloth2* flies were 100% pupal lethal (Figure 8G). However, raising *tub>sloth2* flies at 18˚C, which decreases Gal4/UAS expression, produced escaper adults that had short scutellar bristles (not shown), reminiscent of loss of function of either *sloth1* or *sloth2* (Figure 2K). Hence, an imbalance in complex stoichiometry caused by overexpression of one member of the complex disrupts complex function, and this can sometimes be corrected by coexpression of other members of the complex (CLARK-ADAMS *et al.* 1988). Indeed, we found that *tub>sloth2, sloth1* animals were viable (Figure 8G) and exhibited normal bristles (not shown). Similarly, overexpression of the entire bicistronic transcript had no obvious phenotypes (Figure 8G, not shown). In all, these results support a model whereby Sloth1 and Sloth2 act in a complex in which the stoichiometric ratio is important for normal function.

Discussion

Here, we have assigned new functions to two previously uncharacterized smORF peptides, Sloth1 and Sloth2. *sloth1* and *sloth2* appear to be distantly-related paralogs, yet each is important to support mitochondrial and neuronal function in *Drosophila*. We propose a model where Sloth1 and Sloth2 peptides are translated from the same transcript and imported into the mitochondrial inner membrane, where they form a complex and carry out functions that support ATP production (Figure 9). Our results are supported by a recent study published during preparation of this manuscript, in which human Sloth2 (C12orf73/Brawnin) was described as a mitochondrial component in cultured human cells and zebrafish (ZHANG *et al.* 2020). Importantly, this suggests that human Sloth1 (SMIM4) is also a mitochondrial component in humans.

Muti-cistronic genes are relatively rare in eukaryotes, but some have been characterized in *Drosophila* (GALINDO *et al.* 2007; MAGNY *et al.* 2013) and mammals (KARGINOV *et al.* 2017). Similar to operons in prokaryotes, it is thought that multicistronic transcripts allow for coordinated expression of proteins in the same pathway or complex (KARGINOV *et al.* 2017). Indeed, the similarity of loss of function phenotypes between *sloth1* and *sloth2* suggest that they function together in the same pathway/complex. Interestingly, 44/196 annotated bicistronic genes in *Drosophila* contain two ORFs with homology to each other

(Flybase, DIOPT), and a recent study suggests that human bicistronic genes containing a smORF frequently encode physically interacting peptide/protein pair (CHEN *et al.* 2020). Therefore, related peptides encoded on the same transcript may be a prevalent phenomenon in eukaryotes. ORF translation in multicistronic transcripts can occur by different mechanisms, such as re-initiation of translation, IRES, or leaky ribosome scanning (VAN DER KELEN *et al.* 2009). Our data and observations support leaky scanning, and we propose a model whereby both peptides are translated because *sloth1* contains a non-optimal Kozak sequence.

The presence of *sloth1* and *sloth2* orthologs in many eukaryotic species suggest that their function in fly and humans are likely similar. Indeed, we could rescue the lethality of *sloth1* and *sloth2* mutant flies by expressing their human counterparts. Furthermore, human SMIM4 contains a predicted mitochondrial targeting sequence like Sloth1, human SMIM4 and C12orf73 localize to mitochondria in five human cell lines (THUL *et al.* 2017), and human C12orf73 knockdown leads to impaired mitochondrial respiration in cultured U87MG cells (ZHANG *et al.* 2020). Interestingly, *Plasmodium* and *Arabidopsis* only have homologs with similarity to *sloth2*. This suggests that *sloth2* has maintained functions more similar to its common ancestor with *sloth1*. We were unable to identify homologs in some eukaryotes such as yeast, though their amino acid sequence may simply be too diverged for detection using bioinformatic programs such as BLAST.

Several questions remain with regards to Sloth1 and Sloth2 localization. For example, it is unclear how Sloth2 is trafficked to mitochondria, since it does not have a predicted mitochondrial-sorting signal like Sloth1. It is possible that Sloth2 has a cryptic signal that is not recognized by prediction software, or perhaps it is co-imported with another protein. Furthermore, there are other proteins that are imported into the mitochondria that do not use a classical presequence sorting signal (CHACINSKA *et al.* 2009). Finally, these peptides may play a role outside the cell, since Sloth2 has a predicted secretion signal, and we could detect GFP-tagged Sloth1 and Sloth2 in S2R+ culture media. This phenomenon is not without precedent, as some proteins have been described to localize to both mitochondria and the secretory pathway, such as human SMIM20/Phoenixin (YOSTEN *et al.* 2013), *Drosophila* Stunted (DELANOUE *et al.* 2016), and human MICOS complex subunit MIC26 (KOOB *et al.* 2015).

Sloth1 and Sloth2 likely function together in a complex at the inner mitochondrial membrane. Sloth1 is predicted to localize to the inner membrane based on its domain structure (SAVOJARDO *et al.* 2020), and we found that it physically interacts with Tim8/13, which are chaperones in the intermembrane space that guide import of proteins to the inner membrane. Furthermore, recent proteomics (LIU *et al.* 2018; HANA *et al.* 2020) and cell fractionation (ZHANG *et al.* 2020) studies suggest human C12orf73 localizes to the inner mitochondrial membrane. In addition, we showed that Sloth1 and Sloth2 physically interact. Furthermore, stoichiometric binding in a complex may explain why single mutants have the

same phenotype as double mutants. Many mitochondrial functions are performed at the inner membrane, such as the electron transport chain (ETC), metabolite transport, and cristae formation (STOJANOVSKI *et al.* 2012; KUHLBRANDT 2015). Therefore, considering the defects in ATP production in mutants, it is tempting to speculate that Sloth1 and Sloth2 interact with ETC components such as Complex III (ZHANG *et al.* 2020). Interestingly, ~40 smORF peptides function at the human mitochondrial inner membrane (UniProt), such as the Complex III member UQCRQ (82aa) (USUI *et al.* 1990) and the recently described Mitoregulin/MoxI (56aa) that regulates the electron transport chain and fatty acid β-oxidation (MAKAREWICH *et al.* 2018; STEIN *et al.* 2018; CHUGUNOVA *et al.* 2019). Therefore, modulation of protein complexes in the inner mitochondrial membrane may be a common function of smORF peptides.

Neurons have a high metabolic demand and critically depend on ATP generated from mitochondria to support processes such as neurotransmission (VERSTREKEN *et al.* 2005; KANN AND KOVACS 2007). Therefore, it is not unexpected that neurodegenerative diseases are frequently associated with mitochondrial dysfunction (GOLPICH *et al.* 2017). We find similar results in *Drosophila*, where loss of *sloth1* and *sloth2* leads to defects in mitochondrial function, impaired neuronal function, photoreceptor degeneration, and Rh1 accumulation in photoreceptors. Despite finding that the *Gal4-KI* reporter was strongly expressed in neurons, it is likely these peptides play important roles in other cell types. For example, publicly available RNA-seq data suggest that they are ubiquitously expressed (Flybase). In addition, neuronal expression of *sloth1* or *sloth2* was unable to rescue mutant lethality (not shown).

There is great interest in identifying the complete mitochondrial proteome (CALVO *et al.* 2016), so it is remarkable that *sloth1* and *sloth2* have been largely missed in proteomic or genetic screens for mitochondrial components. Though, recently human C12orf73 was identified in a recent BioID-based proteomics effort (HANA *et al.* 2020). It is possible that the small size of these peptides lead to this discrepancy; due to less frequent mutations in these ORFs, or fewer tryptic products for MS. It is also possible that these peptides form weak interactions with other mitochondrial proteins, preventing their purification during biochemical pull-downs. Indeed, we were unable to identify any interacting mitochondrial proteins other than Tim8/Tim13. At present, there are no reported human disease-associated mutations in *SMIM4* and *C12orf73*. Mutations in these genes might not cause disease, or they might cause lethality. It is also possible that the lack of functional information on these genes has hampered identification of disease-associated mutations.

Our discovery of *sloth1* and *sloth2* highlights the effectiveness of loss of function genetics for identifying smORF genes with important biological functions. Recent technical advances such as genome engineering (e.g. CRISPR/Cas9) and massively parallel profiling have the potential to rapidly assign functions to many uncharacterized smORFs (GUO *et al.* 2018; CHEN *et al.* 2020). For example,

investigation of uncharacterized smORF genes may yield additional important mitochondrial components. Indeed, there is a greater tendency for annotated human smORF peptides to localize to mitochondria (72/719, 10%) compared to the whole proteome (1228/20351, 6%) (UniProt). As functional annotation of hundreds, perhaps thousands, of smORF genes is becoming easier, many new biological insights are likely to emerge from their analyses.

Acknowledgements:

We thank the TRiP and DRSC for help generating transgenic flies, Dr. Marcia Haigis for use of a Seahorse XF analyzer, Claire Hu, Tera Levin, and Dan Richter for bioinformatics help, Lucy Liu for assistance mounting larvae to image the NMJ, and Rich Binari and Cathryn Murphy for general assistance. We thank members of the BDGP for discussions. We also thank the HMS MicRoN (Microscopy Resources on the North Quad) Core. J.A.B. was supported by the Damon Runyon Foundation. This work was supported by NIH grants R01GM084947, R01GM067761, R24OD019847, and NHGRI HG009352 (S.E.C). N.P. is an investigator of the Howard Hughes Medical Institute.

Author Contributions:

Conceptualization, J.A.B., B.U., I.P., B.B., S.C., H.B., N.P.; Methodology, J.A.B., B.U., I.P., N.P.; Investigation, J.A.B., B.U., I.P., J.R., F.E., Z.Z.; Writing – Original Draft, J.A.B.; Writing – Review & Editing, J.A.B., B.U., I.P., J.R., F.E., Z.Z., S.C., H.B., N.P.; Supervision, B.B., S.C., D.S., H.B., N.P.; Funding acquisition, J.A.B., B.B., S.C., N.P.

Declaration of Interests:

The authors declare no competing interests.

Figure titles and legends:

Figure 1: Bicistronic gene structure of the smORFs *sloth1* and *sloth2.* A. Bicistronic gene model for *sloth1* and *sloth2*. Zoom in shows intervening sequence (*GCAAA*) between *sloth1* stop codon and *sloth2* start codon. **B.** Comparison of protein structure, amino acid length size, and amino acid percent identity between *Drosophila* and Human orthologs. Shaded rectangle indicates predicted transmembrane (TM) domain. **C.** Phylogenetic tree of *sloth1* and *sloth2* orthologs in representative eukaryotic species. Linked gene structure (candidate bicistronic transcript or adjacent separate transcripts) is indicated by a black line connecting red and blue squares. **D.** Plasmid reporter structure of *pMT-sloth1-Rluc* and derivatives. Kozak sequences upstream of start codon are underlined. Mutations indicated with shaded grey box. pMT= Metallothionein promoter. RLuc = Renilla Luciferase. **E.** Quantification of RLuc luminescence/Firefly Luciferase, normalized to *pMT-sloth1-Rluc*, for each construct. Significance of mutant

plasmid luminescence was calculated with a T-Test comparing to *pMT-sloth1-Rluc*. Error bars are mean with SEM. **** P≤0.0001. N=4 biological replicates.

Figure 2: *sloth1* and *sloth2* loss of function analysis. A. *sloth1-sloth2* transcript structure with shRNA and sgRNA target locations, primer binding sites, in/del locations, and knock-in Gal4 transgene. **B.** qPCR quantification of RNAi knockdown of the *sloth1-sloth2* transcript. Significance of fold change knockdown was calculated with a T-Test comparing to *da>attP40* for PD43265 and PD43573. Error bars show mean with SEM. P-values *** P≤0.001. N=6. **C.** Quantification of adult fly viability from *sloth1-sloth2* RNAi knockdown. Fly cross schematic (left) and graph (right) with percentage of progeny with or without the CyO balancer. Ratios of balancer to non-balancer were analyzed by Chi square test, **** P≤0.0001. Sample size (N) indicated on graph. **D.** Pictures of fly food vials, focused on the surface of the food. *da>shRNA* flies are frequently found stuck in the fly food. **E.** Quantification of adult fly climbing ability after *sloth1* and *sloth2* RNAi. Significance calculated with a T-test, **** P≤0.0001. Error bars show mean with SD. N=3 biological replicates. **F.** Stereo microscope images of adult fly thorax to visualize the scutellar bristles. RNAi knockdown by *da-Gal4* crossed with either *attP40* or *UAS-shRNA*^{JAB200}*.* Arrowheads point to the two longest scutellar bristles. **G.** Quantification of adult fly viability from *sloth1-sloth2* somatic knockout. Fly cross schematic (left) and graph (right) with percentage of progeny with or without the CyO balancer. Ratios of balancer to non-balancer were analyzed by Chi square test, **** P≤0.0001. Sample size (N) indicated on graph. **H.** (Left) Stereo microscope images of adult fly thorax to visualize the scutellar bristles. Somatic knockout performed by crossing *Act-Cas9* to sgRNAs. (Right) Quantification of the frequency of adult flies with at least one short scutellar bristle after somatic KO of *sloth1* or *sloth2.* Sample sizes indicated on graph. Arrowheads point to the two longest scutellar bristles. **I.** Quantification of adult fly viability from *sloth1-sloth2* hemizygous knockout in males and rescue with a genomic transgene or *UAS-sloth1-sloth2* transgene. Fly cross schematic (left) and graph (right) with percentage of male progeny with or without the FM7c balancer. Sample size (N) indicated on graph. **J.** Still images from video of adult flies inside plastic vials. Images are 5 seconds after vials were tapped. Adult flies climb upward immediately after tapping. All flies are males. Each vial contains 10 flies, except dKO, which contains 5 flies. **K.** Stereo microscope images of adult male fly thorax to visualize the scutellar bristles. *attP40* is used as a negative control. Arrowheads point to the two longest scutellar bristles. **L.** Hemizygous mutant male genetic rescue experiments.

Figure 3. *sloth1-sloth2* are expressed in neurons A. Fluorescent stereo microscope images of 3rd instar larvae expressing GFP with indicated genotypes. **B.** Fluorescent compound microscope image of 3rd instar larval brain expressing *UAS-GFP*. DAPI staining labels nuclei. **C.** Confocal microscopy of adult brain with indicated genotypes. Anti-HRP staining labels neurons. **D.** Confocal microscopy of the 3rd instar larval NMJ at muscle 6/7 segment A2 expressing *UAS-GFP*. Anti-FasII staining labels the entire NMJ. **E.** Confocal microscopy of

the 3rd instar larval ventral nerve cord (VNC) expressing *Gal4-KI*, *UAS-GFP-nls*. GFP-nls is localized to nuclei. Anti-Elav stains nuclei of neurons. Arrow indicates example nuclei that expresses UAS-GFP and is positive for Elav.

Figure 4. *sloth1-sloth2* are important for neuronal function. A. Traces of electrical recordings from 3rd instar larval NMJ in control, *dKO*, and *dKO+genomic rescue* animals over 10 minutes under high frequency stimulation (10 Hz). Graph on right is a quantification of the relative excitatory junction potential (EJP) for indicated genotypes. Error bars show mean with SD. N ≥ 5 larvae per genotype. Significance for each genotype was calculated with a T-Test comparing to control flies. **B-D.** Traces of electroretinogram (ERG) recordings from adult eye photoreceptors upon repetitive stimulation with light (left) and quantification of the relative ERG amplitude for indicated genotypes (right). Error bars show mean with SD. N ≥ 6 larvae per genotype. ** P≤0.01, *** P≤0.001. Significance for each genotype was calculated with a T-Test comparing to control flies. **B.** Recordings were taken from 1-3 days post-eclosion animals that were raised in a 12hr light/dark cycle. “On” and “Off” transients indicated by closed and open arrowhead, respectively. **C.** Recordings were taken from 1-3 days post-eclosion animals that were raised in a 24hr dark. **D.** Recordings were taken from four week aged animals that were raised in a 12hr light/dark cycle.

Figure 5. Loss of *sloth1-sloth2* causes neurodegeneration. A-C. Transmission electron microscopy (TEM) images of sectioned adult eye photoreceptors (left) and quantification of photoreceptor number and aberrant photoreceptors (right). Scalebar is 2μm. Filled red arrows indicate dead or dying photoreceptors. Open red arrows indicate unhealthy photoreceptors. Error bars show mean with SD. N ≥ 8 ommatidium per genotype. **A.** 4 weeks old raised in a 12hr light/dark cycle. **B.** 3 days old raised in a 12hr light/dark cycle. **C.** 4 weeks old raised in 24hr dark. **D.** Confocal microscopy of adult eye photoreceptors stained with phalloidin (green) and anti-Rh1 (red). Animals were 4 weeks old and raised in a 12hr light/dark cycle. Arrowheads indicate photoreceptors with higher levels of Rh1.

Figure 6. Sloth1 and Sloth2 localize to mitochondria. A. Analysis of fly and human Sloth1 and Sloth2 using subcellular localization prediction software. **B.** Amino acid alignment of the N-terminal portion of Sloth1 and Sloth2 orthologs with indicated predicted domains. **C.** Confocal microscopy of S2R+ cells transfected with Sloth1-FLAG or Sloth2-FLAG and stained with anti-FLAG (green) and anti-ATP5alpha (red). DAPI (blue) stains nuclei. **D.** Schematic of Sloth1 and Sloth2 pulldown experiments, mass spectrometry, and SAINT analysis. **E-G.** Western blots showing results from co-immunoprecipitation experiments. **E.** Sloth1-SBP used as bait to pulldown Tim8-HA. **F.** Sloth1-SBP used as bait to pulldown Tim13-HA. **G.** Sloth1-SBP or Sloth2-SBP used as bait to pulldown Tim8-HA.

Figure 7. *sloth1-sloth2* are important for mitochondrial function. A. Seahorse mitochondrial stress report for wildtype S2R+ and dKO #1 cells. Error bars show mean with SD. N=6 for each genotype. **B.** Quantification of basal OCR (timepoint 3) in panel A and including data from single KO and additional dKO cell lines. Significance of KO lines was calculated with a T-test compared to S2R+. Error bars show mean with SD. **** P≤0.0001. N=6 for each genotype. **C.** Quantification of ATP levels in 3rd instar larvae. Error bars show mean with SEM. N = 3 experiments. **D.** Western blot from lysates of 3rd instar larval brains. **E-F.** TEM images of sectioned adult photoreceptors (left) and quantification of mitochondria number (right). Mitochondria are indicated with red dots. Error bars show mean with SD. Sample size indicated on graph. **E.** Adult flies are 4 weeks old and raised in a 12hr light/dark cycle. **F.** Adult flies are 3 days old and raised in a 12hr light/dark cycle.

Figure 8. Sloth1 and Sloth2 act in a stoichiometric complex. A-C. Western blots from co-immunoprecipitation experiments. **A-B.** Pulldown using Sloth1-FLAG and Sloth2-FLAG as bait and either Sloth1-HA or Sloth2-HA as prey. **C.** Pulldown using Sloth1-SBP and Sloth2-SBP as bait and Sloth2-HA as prey. **D.** Seahorse mitochondrial stress report for *sloth1* and *sloth2* stably overexpressing cell lines. Cells were incubated with CuSO4 for 16hr to induce expression. Error bars show mean with SD. N=6 for each genotype. **E.** Quantification of basal respiration (timepoint 3) in panel D. Significance of OE lines were calculated with a T-test compared to S2R+. Error bars show mean with SD. ****P≤0.0001. N=6 for each genotype. **F.** Quantification of luminescence (CellTiter Glo) after 5 days incubation without or with CuSO4 to induce expression. For each cell line, luminescence is normalized to $CuSO4^{-}$. Significance of $CuSO4^{+}$ samples was calculated with a T-test compared to $CuSO4^{-}$. Error bars show mean with SD. ****P≤0.0001. N=8 for each genotype. **G.** Summary of in-vivo overexpression experiments. *tub-Gal4* used to overexpress indicated transgenes.

Methods

Molecular cloning

Plasmid DNAs were constructed and propagated using standard protocols. Briefly, chemically competent TOP10 *E.coli.* (Invitrogen, C404010) were transformed with plasmids containing either Ampicillin or Kanamycin resistance genes and were selected on LB-Agar plates with 100µg/ml Ampicillin or 50µg/ml Kanamycin. Oligo sequences are in Supplemental File 2.

sloth1-sloth2 expression reporters: *pMT-sloth1-RLuc* was constructed by Gibson (NEB E2611) assembly of two DNA fragments with overlapping sequence, 1) 5'UTR, *sloth1* coding sequence, and intervening sequence (*GCAAA*) were amplified from S2R+ genomic DNA. 2) Plasmid backbone was amplified from *pRmHa-3-Renilla* (ZHOU *et al.* 2008), which contains a *Metallothionein* promoter

and coding sequence for Renilla luciferase. *pMT-sloth1-RLuc* derivatives were constructed by a PCR-based site directed mutagenesis (SDM) strategy.

shRNA expression vector for in vivo RNAi: *pValium20-sloth1-sloth2* (aka *UAS-shRNA*, or *JAB200*) was constructed by annealing complementary oligos and ligating into *pValium20* (NI *et al.* 2011) digested with NheI and EcoRI. See Supplemental Figure 1 for location of target site.

sgRNA expression vectors for CRISPR/Cas9: Plasmids encoding two sgRNAs were constructed by PCR amplifying an insert and ligating into *pCFD4* (PORT *et al.* 2014) digested with BbsI. sgRNAs constructed: *pCFD4-sloth1* (aka JAB203), *pCFD4-sloth2* (aka GP01169), *pCFD4-sloth1-sloth2* (aka JAB205, for dKO). See Supplemental Figure 1 for location of target sites.
Gal4 HDR donor plasmid: *pHD-sloth1-sloth2-Gal4-SV40-loxP-dsRed-loxP* was assembled by digesting *pHD-DsRed-attP* (GRATZ *et al.* 2014) with EcoRI/XhoI and Gibson assembling with four PCR amplified fragments: 1) Left homology arm from genomic DNA from *nos-Cas9[attP2]* flies. 2) *Gal4-SV40* from *pAct-FRT-stop-FRT3-FRT-FRT3-Gal4 attB* (BOSCH *et al.* 2015). 3) *loxP-dsRed-loxP* from *pHD-DsRed-attP*. 4) Right homology arm from genomic DNA from *nos-Cas9[attP2]* flies.

pEntr vectors: Construction of pEntr vectors (for Gateway cloning) was performed by Gibson assembly of PCR amplified backbone from pEntr-dTOPO (Invitrogen C4040-10) and PCR amplified gene coding sequence (when appropriate, with or without stop codon). List of plasmids: *pEntr_sloth1* (from S2R+ cDNA), *pEntr_sloth2* (from S2R+ cDNA), *pEntr_hSMIM4* (from IDT gBlock), *pEntr_hC12orf73* (from IDT gBlock), *pEntr_sloth1-sloth2* transcript (from S2R+ cDNA), *pEntr_sloth1-sloth2* genomic (from S2R+ genomic DNA), and *pEntr_BFP* (from *mTagBFP2*). Derivatives of *pEntr_sloth1-sloth2* genomic that lack *sloth1* or *sloth2* coding sequence, or derivatives of *pEntr_sloth1* or *pEntr_sloth2* with or without only the N-terminal signal sequence, were generated by PCR amplifying the plasmid and reassembling the linearized plasmid (minus the desired sequence) by Gibson.

Custom gateway expression vectors: *pWalium10-roe-sfGFP* was constructed by digesting *pWalium10-roe* (PERKINS *et al.* 2015) with XbaI and Gibson assembling with *sfGFP* sequence that was PCR amplified from *pUAS-TransTimer* (HE *et al.* 2019). *pMK33-GW* was a gift from Ram Viswanatha. *pMT-GW-SBP* was constructed by digesting *pMK33-SBP-C* (YANG AND VERAKSA 2017) and *pMK33-GW* with XhoI/SpeI and ligating the GW insert into digested *pMK33-SBP-C* using T4 ligase.

Gateway cloning LR reactions: Gateway cloning reactions were performed using LR Clonase II Enzyme mix (Invitrogen 11791-020). See Supplemental File 3 for plasmids constructed by Gateway reactions. Additional plasmids obtained were *pEntr_Tim8_nostop* and *pEntr_Tim13_nostop* (The FlyBi Consortium), *pAWF*

and *pAWH* (Carnegie Science/Murphy lab), *pWalium10-roe* (PERKINS *et al.* 2015), and *pBID-G* (WANG *et al.* 2012).

Fly genetics

Flies were maintained on standard fly food at 25˚C. Wild-type (WT) or control flies refers to *yw*. The *yv; attP40* strain is used as a negative control for experiments involving an shRNA or sgRNA transgene inserted into *attP40*.

Fly stocks were obtained from the Perrimon lab collection, Bloomington Stock center (indicated with BL#), or generated in this study (see below). Bloomington Stocks: *yw* (1495), *yv; P{y[+t7.7]=CaryP}attP40* (36304), *yv,P{y[+t7.7]=nos-phiC31\int.NLS}X; P{y[+t7.7]=CaryP}attP40* (25709), *P{y[+t7.7]=nos-phiC31\int.NLS}X, y[1] sc[1] v[1] sev[21]; P{y[+t7.7]=CaryP}attP2* (25710), *w[1118]; Dp(1;3)DC166, PBac{y[+mDint2] w[+mC]=DC166}VK00033* (30299), *y[1] M{w[+mC]=Act5C-Cas9.P}ZH-2A w[*]* (54590), *y[1] sc[*] v[1] sev[21]; P{y[+t7.7] v[+t1.8]=nos-Cas9.R}attP2* (78782), *w[*]; P{w[+mC]=UAS-2xEGFP}AH2* (6874), *w[1118]; P{w[+mC]=UAS-GFP.nls}14* (4775), *y1 w*; P{tubP-GAL4}LL7/TM3, Sb1 Ser1* (5138), *MN-Gal4*, *UAS-mitoGFP* (42737), *MN-Gal4*, *UAS-nSybGFP* (9263). Perrimon Lab stocks: *w; da-Gal4*, *lethal/FM7-GFP*.

Transgenic flies using PhiC31 integration were made by injecting attB-containing plasmids at 200ng/ul into integrase-expressing embryos that contained an attP landing site (attP40 or attP2). Injected adults were outcrossed to balancer chromosome lines to isolate transgenic founder flies and eventually generate balanced stocks. *pCFD4-sloth1[attP40]* (aka JAB203), *pCFD4-sloth2[attP40]* (aka GP01169), *pCFD4-sloth1-sloth2[attP40]* (aka JAB205, for dKO), *pValium20-sloth1-sloth2[attP40]* (aka *UAS-shRNA*, or *JAB200*) lines were selected with *vermillion+*. *pWalium10-sloth1[attP2]*, *pWalium10-sloth2[attP2]*, *pValium10-sloth2[attP40]*, *pWalium10-hSMIM4[attP2]*, *pWalium10-hC12orf73[attP2]*, *pWalium10-sloth1-sloth2*transcript*[attP2]*, *pBID-{sloth1-sloth2}[attP40]*, *pBID-{Δsloth1-sloth2}[attP40]*, *pBID-{sloth1-Δsloth2}[attP40]* were selected with *white+.*

sloth1-KO, *sloth2-KO,* and *dKO* fly lines were made by crossing sgRNA-expressing transgenic lines to *nos-Cas9[attP2]* flies, outcrossing progeny to *FM7-GFP* balancer flies, and screening progeny founder flies for deletions by PCR and Sanger sequencing.

Gal4-KI flies were made by injecting sgRNA plasmid (JAB205) and *pHD-sloth1-sloth2-Gal4-SV40-loxP-dsRed-loxP*, each at 200ng/ul, into embryos expressing Cas9 in the germ line (*nos-Cas9*). Injected adults were outcrossed to *FM7-GFP* flies, progeny were screened for RFP+ expression, and RFP+ founder lines were confirmed by PCR for a correct knock-in.

Knockdown crosses were performed by crossing *da-Gal4* with *pValium20-sloth1-sloth2[attP40]/CyO* (aka *UAS-shRNA*, or *JAB200*) or *attP40/CyO* as a negative control. Quantification of viability was performed by counting the number of progeny with or without the CyO balancer. A Chi-square test was used to determine if the ratio of non-balancer flies (CyO^-) to balancer flies (CyO^+) was significantly altered in shRNA crosses compared to control crosses. Data was analyzed using Excel and Prism.

For climbing assays, *da-Gal4/shRNA or da-Gal4/attP40* adult progeny were aged 1 week after eclosion and 10 flies were transferred into empty plastic vials without use of CO2. Climbing ability was quantified by tapping vials and recording the number of flies that climb to the top of the vial within 10 seconds, using video analysis. Climbing assays with the same 10 flies were performed three times and averaged. Three biological replicates were performed for each genotype. A T-Test was used to calculate statistical significance. Data was analyzed using Excel and Prism.

Somatic knockout crosses were performed by crossing *Act-Cas9* to *sgRNA[attP40]/CyO* or *attP40/CyO* as a negative control. *Act-Cas9/sgRNA[attP40]* female and male progeny were analyzed for phenotypes. Quantification of viability was performed by counting the number of progeny with or without the *CyO* balancer. A Chi-square test was used to determine if the ratio of non-balancer flies (CyO^-) to balancer flies (CyO^+) was significantly altered in somatic knockout crosses compared to control crosses. Male and female progeny were analyzed separately because they differ in the number of copies of the endogenous *sloth1-sloth2* loci on the X-chromosome. Data was analyzed using Excel and Prism.

Mutant and genomic rescue crosses were performed by crossing *mutant/FM7-GFP* females to genomic rescue constructs or *attP40* as a negative control. *mutant/Y* hemizygous male progeny were analyzed for phenotypes. Quantification of viability was performed by counting the number of *mutant/Y* vs *FM7GFP* male progeny. Gal4/UAS rescue crosses were performed by crossing *mutant/FM7-GFP;; da-Gal4* females to *UAS-X* lines. Additionally, *Gal4-KI/FM7-GFP* females were crossed to UAS-X. Rare *sloth1*-KO, *sloth2-KO, dKO,* and *Gal4-KI* hemizygous adult males normally die by sticking to the fly food after they eclose. To collect these rare mutants for further analysis (scutellar bristle images, climbing assays), we inverted progeny vials so that mutant adults fell onto the dry cotton plug once they eclose.

Overexpression crosses were performed by crossing *tub-Gal4/TM3* females to *UAS-X* lines. *tub-Gal4/UAS-X* progeny were analyzed for phenotypes. Quantification of viability was performed by counting the number females and males with and without *TM3*. A Chi-square test was used to determine if the ratio of non-balancer flies ($TM3^-$) to balancer flies ($TM3^+$) was significantly altered in

963 overexpression crosses compared to control crosses. Data was analyzed using
964 Excel and Prism.
965
966 **Cell culture**
967
968 *Drosophila* S2R+ cells (YANAGAWA *et al.* 1998), or S2R+ cells stably expressing
969 Cas9 and a mCherry protein trap in *Clic* (known as PT5/Cas9) (VISWANATHA *et al.*
970 2018), were cultured at 25˚C using Schneider's media (21720-024,
971 ThermoFisher) with 10% FBS (A3912, Sigma) and 50 U/ml penicillin strep
972 (15070-063, ThermoFisher). S2R+ cells were transfected using Effectene
973 (301427, Qiagen) following the manufacturer's instructions.
974
975 For generating stable cell lines, S2R+ cells were seeded in 6-well plates and
976 transfected with *pMK33* expression plasmids (see Supplemental File 3). *pMK33*
977 derived plasmids contain a Hygromycin resistance gene and a *Metallothionein*
978 promoter to induce gene expression. After 4 days, transfected cells were
979 selected with 200µg/ml Hygromycin in Schneider's medium for approximately 1
980 month. For induction of gene expression, cells were cultured with 500 µM CuSO4
981 in Schneider's medium for 16hrs for Seahorse and pulldown/MS experiments, or
982 indefinitely for viability experiments.
983
984 For generating KO cell lines, S2R+Cas9 cells were transfected with *tub-GFP*
985 plasmid (gift of Steve Cohen) and an sgRNA-expressing plasmid (*pCFD4-*
986 *sloth1[attP40]* (aka JAB203), *pCFD4-sloth2[attP40]* (aka GP01169), or *pCFD4-*
987 *sloth1-sloth2[attP40]* (aka JAB205, for dKO)). 48hrs after transfection, cells were
988 resuspended in fresh media, triturated to break up cell clumps, and pipetted into
989 a cell straining FACS tube (352235 Corning). Single GFP+ cells were sorted into
990 single wells of a 96 well plate containing 50% conditioned media using an Aria-
991 594 instrument at the Harvard Medical School Division of Immunology's Flow
992 Cytometry Facility. Once colonies were visible by eye (3-4 weeks), they were
993 expanded and analyzed by PCR and Sanger sequencing.
994
995 For quantification of S2R+ cell viability, CellTiter-Glo (Promega, G7570) was
996 used following the manufacturer's instructions. Briefly, wild-type S2R+ cells, or
997 stable S2R+ cells, were seeded into opaque bottom 96 well plates at 10,000
998 cells/well and CuSO4 was added at 500µM final concentration. After five days of
999 incubation at 25˚C, 50µl of CellTiter-Glo reagent was added to each well,
1000 incubated for 10min on an orbital shaker, and luminescence recorded (Molecular
1001 Devices Spectramax Paradigm). N=8 wells per condition. Significance as
1002 calculated using a T-Test.
1003
1004 For co-immunoprecipitation experiments, S2R+ cells were transfected in 6-well
1005 dishes. Three days after transfection, CuSO4 was added at 500µM (to induce
1006 expression from *pMK33* plasmids), Four days after transfection, cells were
1007 resuspended and centrifuged at 150g for 10min. Cell pellets were washed once
1008 with 1x PBS and re-centrifuged. Cell pellets were lysed by resuspending in 500µl

IP Lysis Buffer (Pierce 87788) and allowing to sit on ice for 20min. Cell lysates were centrifuged at 12,000g at 4˚C for 10min. Each supernatant was transferred to a new tube and incubated with either 40µl anti-FLAG agarose beads (Sigma-Aldrich M8823) or 40µl magnetic streptavidin beads (Pierce 88817) for 4hr at 4˚C. Beads were washed three times in lysis buffer and boiled in 2x SDS Sample Buffer (anti-FLAG pulldowns) or 3x SDS Sample Buffer with 2mM biotin and 20mM DTT (streptavidin pulldowns) for analysis by western blotting.

For large-scale pull-down experiments, we followed a previously described protocol (YANG AND VERAKSA 2017) with some modifications. Briefly, each cell line (S2R+, MT-BFP-SBP, MT-Sloth1-SBP, MT-Sloth2-SBP) was grown in T175 flasks (30ml). 16hr before collection, CuSO4 was added at 70µM. Cells were pelleted at 500g for 5min at 4˚C, washed with 1x cold PBS, and re-centrifuged. Cell pellets were lysed in 1ml lysis buffer (50mM Tris pH 7.5, 5% Glycerol, .2% IGEPAL, 1.5mM MgCl2, 125mM NaCl, 25mM NaF, 1mM Na3VO4, 1mM DTT, 1x Halt Protease Inhibitor Pierce 87786) by pipetting up and down and incubated on ice for 20min. Cell lysates were centrifuged at 14,000g for 15min at 4˚C. Supernatants were filtered (.45µm) and incubated with 300µl streptavidin beads for 3 hours at 4˚C rotating. Using a magnetic stand (Bio-Rad 1614916), beads were collected and washed with lysis buffer five times. Proteins were eluted by suspending beads in 100µl 2mM biotin solution (1:100 dilution of 200mM biotin in 2 M NH4OH, diluted in lysis buffer) and incubating on ice for 5min. Using a magnetic stand, the elution was transferred to a new tube. Elutions were repeated two additional times to result in 300µl eluted proteins for each sample. Eluted proteins were isolated by TCA precipitation and submitted for analysis by mass spectrometry at the Beth Israel Deaconess Medical Center Mass Spectrometry Facility. SAINT analysis (CHOI *et al.* 2011) was used to define significant proteomic hits as having a score greater than 0.8.

To assay protein secretion in cell culture media, S2R+ cells were transfected with *Act-Gal4* (Y. Hiromi) and a *UAS-X-sfGFP* plasmid in 24-well plates. Four days after transfection, 100µl media was gently transferred to a centrifuge tube. The remaining cells were resuspended, pelleted at 150g for 10min at 4˚C, washed once with 1xPBS, re-centrifuged, and lysed by boiling in 100µl 2x SDS Sample Buffer. 100µl media was centrifuged at 100g for 10min at 4˚C and 50µl of supernatant was transferred to a new centrifuge tube, mixed with 50µl 4x SDS Sample Buffer, and boiled for 10min.

To measure mitochondrial respiration in S2R+ cells, we performed a Mito Stress Test on a Seahorse XFe96 Analyzer (Agilent, 103015-100). 50,000 cells were seeded into Seahorse XF96 tissue culture microplates and incubated at 25˚C overnight. 1hr before analysis, cell culture media was replaced with serum-free Schneider's media and drugs were loaded into the Seahorse XFe96 Sensor Cartridge (Final concentrations: Oligomycin 1µM, Bam15 .5µM, 1µM Antimyzin/Rotenone "R/A"). Seahorse analysis was performed at room temperature. Mitochondrial respiration recordings were normalized to cell number

using CyQUANT (Thermo Fisher C7026) fluorescence on a plate reader. Data analysis was performed using Seahorse Wave Desktop Software 2.6, Excel, and Prism. N=6 wells for each condition. Significance was calculated using a T-Test.

To measure *MT-sloth1-RLuc* reporter expression, S2R+ cells were transfected in white opaque-bottom 96 well plates with *MT-sloth1-RLuc* (or derivatives) and *MT-FLuc* (Firefly Luciferase) (ZHOU *et al.* 2008) as an internal control. Briefly, to each well, 10ng of plasmid mix was added, then 10µl Enhancer mix (.8µl Enhancer + 9.2µl EC buffer), and was incubated for 2-5min at room temperature. 20µl of Effectene mix (2.5µl Effectene + 17.5µl EC buffer) was added and incubated for 5-10min at room temperature. 150µl of S2R+ cells (at 3.3x10^5 cells/ml) was added gently to each well and incubated at 25˚C. After 3 days incubation, 200µM CuSO4 was added. After 24 hours incubation, media was gently removed from the wells by pipetting and cell luminescence was measured using the Dual-Glo assay (Promega E2920). Two luminescence normalizations were performed. First, for each sample, Renilla luminescence was normalized to Firefly luminescence (Rluc/Fluc). Next, Rluc/Fluc ratios for each sample were normalized to Rluc/Fluc ratios for wild-type *MT-sloth1-RLuc* (aka fold change Rluc/Fluc to WT). For each genotype, N=4. Significance was calculated using a T-test. Data was analyzed using Excel and Prism.

Western blotting

Protein or cell samples were denatured in 2x SDS Sample buffer (100mM Tris-CL pH 6.8, 4% SDS, .2% bromophenol blue, 20% glycerol, .58 M β-mercaptoethanol) by boiling for 10 min. Denatured proteins and Pageruler Prestained Protein Ladder (Thermo Fisher Scientific 26616) were loaded into 4–20% Mini-PROTEAN TGX gels (Biorad 4561096) and ran at 100-200V in a Mini-PROTEAN Tetra Vertical Electrophoresis Cell (Biorad 1658004) using running buffer (25 mM Tris, 192 mM glycine, 0.1% SDS, pH 8.3). Proteins were transferred to Immobilon-FL PVDF (Millipore IPFL00010) in transfer buffer (25 mM Tris, 192 mM glycine) using a Trans-Blot Turbo Transfer System (Biorad 1704150) (Standard SD program). Resulting blots were incubated in TBST (1x TBS + .1% Tween20) for 20min on an orbital shaker, blocked in 5% non-fat milk in TBST, and incubated with primary antibody diluted in blocking solution overnight at 4˚C. Blots were washed with TBST and incubated in secondary antibody in blocking solution for 4 hours at room temperature. Blots were washed in TBST before detection of proteins. HRP-conjugated secondary antibodies were visualized using ECL (34580, ThermoFisher). Blots were imaged on a ChemiDoc MP Imaging System (BioRad)**.**

For western blots from larval brains, 3rd instar larval brains were dissected in ice cold PBS buffer with protease and phosphatase inhibitors. 10 brains per genotype were homogenized in RIPA buffer and protein concentration was measured by BCA assay (Thermo Fischer, 23227). Equal amounts of protein samples were mixed with 1X Sample buffer (BioRad, 161-0747), boiled for 5 min,

and loaded into 4-20% Mini-PROTEAN® TGX gel (Bio-Rad). Gels were then transferred to nitrocellulose membranes using Bio-Rad Trans-Blot SD Semi-Dry Transfer system. Western blots using anti-Hsp60 likely recognize Hsp60A, as opposed to Hsp60B/C/D, because only Hsp60A is expressed in the larval brain (flyrnai.org/tools/dget/web).

Antibodies used for western blotting: rat anti-HA (1:2000, Roche 11867423001), mouse anti-FLAG (1:1000, Sigma F1804), mouse anti-SBP (1:1000, Santa Cruz sc-101595), mouse anti-a-Tubulin (1:20000, Sigma T5168), rabbit anti-GFP (1:5000, Invitrogen A-6455), mouse anti-Cherry (1:3000, Abcam ab167453), rabbit anti-Hsp60 antibody (Abcam ab46798), mouse anti-actin C4 (MP Biomedicals 08691002), anti-mouse HRP (1:3000, NXA931, Amersham), anti-rat HRP (1:3000, Jackson 112-035-062), anti-rabbit HRP (1:3000, Amersham NA934)

Molecular biology

S2R+ cell genomic DNA was isolated using QuickExtract (QE09050, Lucigen). Fly genomic DNA was isolated by grinding a single fly in 50µl squishing buffer (10 mM Tris-Cl pH 8.2, 1 mM EDTA, 25 mM NaCl) with 200µg/ml Proteinase K (3115879001, Roche), incubating at 37˚C for 30 min, and 95˚C for 2 minutes. PCR was performed using Taq polymerase (TAKR001C, ClonTech) when running DNA fragments on a gel, and Phusion polymerase (M-0530, NEB) was used when DNA fragments were sequenced or used for molecular cloning. DNA fragments were run on a 1% agarose gel for imaging or purified on QIAquick columns (28115, Qiagen) for sequencing analysis. Sanger sequencing was performed at the DF/HCC DNA Resource Core facility and chromatograms were analyzed using Lasergene 13 software (DNASTAR).

For RT-qPCR analysis of *sloth1-sloth2* RNAi knockdown, *da-Gal4* was crossed with *attP40* or *UAS-shRNA* and ten 3rd instar larvae progeny of each genotype were flash frozen in liquid nitrogen. Frozen larvae were homogenized in 600µl Trizol (Invitrogen 15596026) and RNA extracted using a Direct-zol RNA Miniprep kit (Zymo Research, R2050). cDNA was generated using the iScript Reverse Transcription Supermix (BioRad 1708840). cDNA was analyzed by RT-qPCR using iQ SYBR Green Supermix (BioRad 170-8880). qPCR primer sequences are listed in Supplemental File 2. Each qPCR reaction was performed with two biological replicates, with three technical replicates each. Data was analyzed using Bio-Rad CFX Manager, Excel, and Prism. Data from *sloth1-sloth2* specific primers were normalized to primers that amplify *GAPDH* and *Rp49*. Statistical significance was calculated using a T-Test.

Bioinformatic analysis

Protein similarity between fly and human Sloth1 and Sloth2 orthologs was determined using BLASTP (blast.ncbi.nlm.nih.gov) by defining the percent amino acid identity between all four comparisons. Homologs in other organisms and

their gene structure were identified using a combination of BLASTP, Ensembl (www.ensembl.org), HomoloGene (www.ncbi.nlm.nih.gov/homologene), and DIOPT (www.flyrnai.org/diopt). Protein accession numbers: Human *SMIM4* NP_001118239.1, Human *C12orf73* NP_001129042.1, Mouse *SMIM4* NP_001295020.1, Mouse *C12orf73 homolog* NP_001129039.1, Zebrafish *SMIM4* NP_001289975.1, Zebrafish *C12orf73 homolog* NP_001129045.1, Lamprey *SMIM4* XP_032827557.1, Lamprey *C12orf73 homolog* XP_032827559.1, *D.melanogaster CG32736* NP_727152.1, *D.melanogaster CG42308* NP_001138171.1, *Arabidopsis AT5G57080* NP_200518.1, *Arabidopsis AT4G26055* NP_001119059.1, *Plasmodium PF3D7_0709800* XP_002808771.1, Choanoflagellate (*Salpingoeca urceolata*) *m.92763* (RICHTER *et al.* 2018), Choanoflagellate (*Salpingoeca urceolata*) *sloth2* homolog is unannotated but present in comp15074_c0_seq2 (RICHTER *et al.* 2018). Sea squirt (*C. intestinalis*) *sloth1* and *sloth2* homologs are unannotated but present in *LOC100183920* XM_018812254.2. Genomic sequences for *sloth1/2* ORFs in *D.melanogaster*, Lamprey, Choanoflagellate, and Sea squirt are shown in Supplemental File 1.

Amino acid sequence of fly and human Sloth1/Sloth2 were analyzed for predicted domains using the following programs: TargetP 2.0 (www.cbs.dtu.dk/services/TargetP), DeepLoc (http://www.cbs.dtu.dk/services/DeepLoc/), PSORT (https://wolfpsort.hgc.jp/), Busca (http://busca.biocomp.unibo.it/), MitoFates (http://mitf.cbrc.jp/MitoFates/cgi-bin/top.cgi), iPSORT (http://ipsort.hgc.jp/), MitoProtII (https://ihg.gsf.de/ihg/mitoprot.html), DeepMito (http://busca.biocomp.unibo.it/deepmito/), PrediSi (http://www.predisi.de/), Phobius (http://phobius.sbc.su.se/), SignalP-5.0, (http://www.cbs.dtu.dk/services/SignalP/), TMHMM 2.0 (http://www.cbs.dtu.dk/services/TMHMM/)

Amino acid sequences were aligned using Clustal Omega (https://www.ebi.ac.uk/Tools/msa/clustalo/) and visualized using Jalview (https://www.jalview.org/).

Imaging

For imaging adult scutellar bristles, adult flies were frozen overnight and dissected to remove their legs and abdomen. Dissected adults were arranged on a white surface and a focal stack was taken using a Zeiss Axio Zoom V16. Focal stacks were merged using Helicon Focus 6.2.2.

For imaging larval brains, wandering 3rd instar larvae were dissected in PBS and carcasses were fixed in 4% paraformaldehyde for 20min. Fixed carcasses were either mounted on slides in mounting medium (see below), or permeabilized in PBT, blocked for 1hr in 5% normal goat serum (S-1000, Vector Labs) at room temperature, and incubated with primary antibody (anti-Elav) overnight at 4˚C, washed with PBT, incubated with secondary antibody (anti-mouse 633) for 4hr at

room temperature, washed with PBT and PBS, and incubated in mounting media (90% glycerol + 10% PBS) overnight at 4˚C. Larval brains were dissected from carcasses and mounted on a glass slide under a coverslip using vectashield (H-1000, Vector Laboratories Inc.). Images of larval brains were acquired on a Zeiss Axio Zoom V16 or a Zeiss 780 confocal microscope. Images were processed using Fiji software.

For imaging the larval NMJ, wandering 3rd instar larvae were dissected as previously described (BRENT *et al.* 2009). Briefly, larvae were pinned to a Sylgard-coated (Dow 4019862) petri dish, an incision was made along their dorsal surface, their cuticle was pinned down to flatten the body wall muscles, and were fixed in 4% paraformaldehyde for 20min. Fixed carcasses were permeabilized in PBT, blocked for 1hr in 5% normal goat serum (S-1000, Vector Labs) at room temperature, and incubated with primary antibody overnight at 4˚C, washed with PBT, incubated with secondary antibody for 4hr at room temperature, washed with PBT and PBS, and incubated in mounting media (90% glycerol + 10% PBS) overnight at 4˚C. Whole carcasses mounted on a glass slide under a coverslip using vectashield (H-1000, Vector Laboratories Inc.). Images of the NMJ were acquired on a Zeiss Axio Zoom V16 or a Zeiss 780 confocal microscope. Images were taken from muscle 6/7 segment A2. Images were processed using Fiji software. Quantification of bouton number from NMJ stained with anti-HRP and anti-Dlg1 was performed by manual counting of boutons in an entire NMJ for wild-type (N=8) and dKO animals (N=7). A T-test was used to determine significance.

For imaging whole larvae, wandering 3rd instar larvae were washed with PBS and heat-killed for 5min on a hot slide warmer to stop movement. Larvae were imaged using a Zeiss Axio Zoom V16 fluorescence microscope.

For imaging the adult brain, ~1 week old adult flies were dissected in PBS and whole brains were fixed in 4% paraformaldehyde for 20min. Fixed brains were permeabilized in PBT, blocked for 1hr in 5% normal goat serum (S-1000, Vector Labs) at room temperature, incubated with anti-HRP 647 overnight at 4˚C, washed with PBT and PBS, and incubated in mounting media (90% glycerol + 10% PBS) overnight at 4˚C. Adult brains were mounted on glass slides under a coverslip using vectashield (H-1000, Vector Laboratories Inc.). Images of adult brains were acquired on a Zeiss 780 confocal microscope. Images were processed using Fiji software.

For confocal microscopy of adult photoreceptors, the proboscis was removed and the head was pre-fixed with 4% formaldehyde in PBS for 30 min. After pre-fixation, eyes were removed from the head and fixed an additional 15 minutes. Fixed eyes were washed with PBS 3x for 10 min each and permeabilized in 0.3% Triton X-100 in PBS for 15 min. Permeabilized, fixed samples were blocked in 1X PBS containing 5% normal goat serum (NGS) and 0.1% Triton X-100 for 1 h (PBT). Samples were incubated in primary antibody diluted in PBT overnight at

4°C, washed 3x with PBT, and incubated in secondary antibodies in NGS for 1hr at room temp the next day. Following secondary antibody incubation, samples were washed with PBS and were mounted on microscope slides using vectashield. Samples were imaged with LSM710 confocal with 63X objective and processed using Fiji software.

S2R+ cells transfected with Sloth1-FLAG or Sloth2-FLAG were plated into wells of a glass-bottom 384 well plate (6007558, PerkinElmer) and allowed to adhere for 2 hours. Cells were fixed by incubating with 4% paraformaldehyde for 30min, washed with PBS with .1% TritonX-100 (PBT) 3x 5min each, blocked in 5% Normal Goat Serum (NGS) in PBT for 1hr at room temperature, and incubated in primary antibodies diluted in PBT-NGS overnight at 4˚C on a rocker. Wells were washed in PBT, incubated with secondary antibodies and DAPI and washed in PBS. Plates were imaged on an IN Cell Analyzer 6000 (GE) using a 20x or 60x objective. Images were processed using Fiji software.

List of antibodies and chemicals used for tissue staining: rat anti-Elav (1:50, DSHB, 7E8A10), goat anti-HRP 647 (1:400, Jackson Immunoresearch, 123-605-021), mouse anti-ATP5α (1:500, Abcam, ab14748), DAPI (1:1000, Thermo Fisher, D1306), rabbit anti-FLAG (1:1000, Sigma, F7425), mouse anti-FasII (1:25, DSHB, 1D4), mouse anti-brp (1:25, DSHB, nc82), mouse anti-Dlg1 (1:250, DSHB, 4F3), anti-mouse 633 (1:500, A-21052, Molecular Probes), mouse monoclonal anti-Rh1 (1:50, DSHB 4C5), Phalloidin conjugated with Alexa 488 (1:250, Invitrogen A12379).

Transmission electron microscopy (TEM) of adult photoreceptors

TEM of *Drosophila* adult retinae were performed following standard electron microscopy procedures using a Ted Pella Bio Wave processing microwave with vacuum attachments. Briefly, whole heads were dissected in accordance to preserve the brain tissue. The tissue was covered in 2% paraformaldehyde, 2.5% Glutaraldehyde, in 0.1 M Sodium Cacodylate buffer at pH 7.2. After dissection, the heads were incubated for 48hrs in the fixative on a rotator at 4˚C. The pre-fixed heads were washed with 3X millipore water followed by secondary fixation with 1% aqueous osmium tetroxide, and rinsed again 3X with millipore water. To dehydrate the samples, concentrations from 25%–100% of Ethanol were used, followed by Propylene Oxide (PO) incubation. Dehydrated samples are infiltrated with gradual resin:PO concentrations followed by overnight infiltration with pure resin. The samples were embedded into flat silicone molds and cured in the oven at 62°C for 3-5 days, depending on the atmospheric humidity. The polymerized samples were thin-sectioned at 48-50 nm and stained with 1% uranyl acetate for 14 minutes followed by 2.5% lead citrate for two minutes before TEM examination. Retina were viewed in a JEOL JEM 1010 transmission electron microscope at 80kV. Images were captured using an AMT XR-16 mid-mount 16 mega-pixel digital camera in Sigma mode. Three animals per genotype per condition were used for TEM. At least 30 photoreceptors were used for organelle

quantifications. Quantification of photoreceptor number, number of aberrant photoreceptors, and number of mitochondria per photoreceptor, was performed in Prism. Significance was calculated using a T-Test.

Electrical recordings

Intracellular Recording from Larval NMJ

3rd instar larval NMJ recordings were performed as described previously (UGUR *et al.* 2017). Briefly, free moving larvae are dissected in HL3.1 buffer without Ca^{2+}. Recordings were performed by stimulating the segmental nerve innervating a hemisegment A3, Muscle 6/7 through a glass capillary electrode filled with HL3.1 with 0.75 mM Ca^{2+}. There were no differences in input resistance, time constant τ, and resting membrane potential among different genotypes tested. Repetitive stimulations were performed at 10Hz and were reported relative to the first excitatory junction potential (EJP). Data were processed with Mini Analysis Program by Synaptosoft, Clampfit, and Excel. At least 5 animals were used per each genotype per essay. Significance was calculated using a T-Test.

Electroretinograms (ERGs)

ERGs were recorded according to (JAISWAL *et al.* 2015). Briefly, flies were immobilized on a glass slide with glue. Glass recording electrodes, filled with 100 mM NaCl, were placed on the surface of the eye to record field potential. Another electrode placed on the humerals served as a grounding electrode. Before recording ERGs, flies were adjusted to darkness for three minutes. Their response to light was measured in 1sec. intervals for 30 sec. To test if the flies can recover from repetitive stimulation, we recorded ERGs after 30 sec. and 1min constant darkness following repetitive stimulation. Data were processed with AXON-pCLAMP8.1. At least 6 animals were used per each genotype per essay. Significance was calculated using a T-Test.

Measurement of ATP levels from larvae

Ten 3rd instar larvae were snap frozen with liquid nitrogen in a 1.5 mL centrifuge tube. Following freezing, samples were homogenized in 100 µl of 6 M guanidine-HCl in extraction buffer (100 mM Tris and 4 mM EDTA, pH 7.8) to inhibit ATPases, and boiled for 3 min. The samples were centrifuged to remove cuticle. Supernatant was serially diluted with extraction buffer and protein concentration was measured using a BCA kit (Thermo Fischer, 23227). For each genotype, ATP levels were measured from equal protein amounts using an Invitrogen ATP detection kit (Invitrogen, A22066) according to their protocol. N=3 experiments, biological triplicates per genotype per experiment. Significance was calculated using a T-Test.

Supplemental Information titles and legends

Supplemental Figure 1: Related to Figure 2. A. Extended gene structure of *sloth1* and *sloth2* and genetic reagents. **B.** Sequence analysis of KO, dKO, and Gal4-KI alleles. **C.** (Left) Diagram of HDR knock-in of Gal4 into the *sloth1-sloth2* locus. (Right) DNA gel confirming Gal4 knock-in by PCR primers that flank the homology arms. Expected DNA fragment size in parenthesis.

Supplemental Figure 2. Related to Figure 4. Traces of electrical recordings from 3rd instar larval NMJ in *dKO*, and *dKO+genomic rescue* animals. Graph on right is a quantification of the excitatory junction potential (EJP) for indicated genotypes. Significance was calculated with a T-Test compared to the *yw* control sample. Error bars show mean with SD. N ≥ 5 larvae per genotype.

Supplemental Figure 3. Related to Figure 5. Confocal microscopy images of 3rd instar larval NMJ at muscle 6/7 segment A2. Antibodies or fluorescent proteins (green) mark synaptic components and anti-HRP (red) marks neurons. Comparison of wild-type to dKO. Graph shows quantification of synaptic bouton number by anti-Dlg1 staining. Significance of dKO bouton number was calculated with a T-test compared to WT. Error bars show mean with SD. N ≥ 7 NMJs (each from a different animal).

Supplemental Figure 4. Related to Figure 5. A-C. Transmission electron microscopy (TEM) images of sectioned adult eye photoreceptors from indicated genetic backgrounds with accompanying quantification of photoreceptor number and aberrant photoreceptors. Scalebar is 2μm. Filled red arrows indicate dead or dying photoreceptors. Open red arrows indicate unhealthy photoreceptors. Error bars show mean with SD. **A.** Animals were 4 weeks old and raised in a 12hr light/dark cycle. **B.** Animals were 1-3 days old and raised in a 12hr light/dark cycle. **C.** Animals were 4 weeks old and raised in the dark.

Supplemental Figure 5. Related to Figure 5. Confocal microscopy of adult eye photoreceptors stained with phalloidin (green) and anti-Rh1 (red). Animals were 4 weeks old and raised in the dark. Arrows indicate photoreceptors with higher levels of Rh1.

Supplemental Figure 6. Related to Figure 6. A-B. Western analysis of cell culture media or cell pellets from transfected S2R+ cells. *Act-Gal4* was co-transfected with indicated *UAS*-plasmids. **A.** Secretion analysis of Sloth1. **B.** Secretion analysis of Sloth2.

Supplemental Figure 7. Related to Figure 7. A. Sequence analysis of single KO S2R+ clones for *sloth1* (clone 2F8) and *sloth2* (clone 3A7). sgRNA and PAM site indicated by grey boxes. **B.** PCR genotyping of four independently derived single cell dKO S2R+ clones. **C-D.** Seahorse mitochondrial stress test quantification of **C.** ATP production and **D.** Proton leak. Significance of KO lines was calculated with a T-test compared to S2R+. Error bars show mean with SD. ** P≤0.01, *** P≤0.001, **** P≤0.0001. N=6 for each genotype. **E.** Confocal

images of 3rd instar larval ventral nerve cord (VNC), axon bundles, and neuromuscular junction (NMJ). *MN-Gal4 UAS-mitoGFP* (*MN>mitoGFP*) (GFP) expresses mitochondrial-localized GFP in motor neurons. Neurons are stained with anti-HRP (magenta).

Supplemental Figure 8. Related to Figure 7. A-B. TEM images of sectioned adult photoreceptors. **A.** Adult flies are 4 weeks old and raised on a 12hr light/dark cycle. Mitochondria are indicated with red dots. **B.** Adult flies are 3 days old and raised in a 12hr light/dark cycle.

Supplemental Figure 9. Related to Figure 8. A-B. Seahorse mitochondrial stress test quantification of Figure 8D. Significance of OE lines was calculated with a T-test compared to S2R+. Error bars show mean with SD. ****P≤0.0001. N=6 for each genotype. **A.** ATP production and **B.** Proton leak.

Supplemental File 1. Genomic sequence of *sloth1-sloth2* homologs in *D. melanogaster*, *S. urceolata*, *P. marinus*, and *C. intestinalis*

Supplemental File 2. Oligo and dsDNA sequenences

Supplemental File 3. Gateway cloning plasmid list

References:

Alloway, P. G., L. Howard and P. J. Dolph, 2000 The formation of stable rhodopsin-arrestin complexes induces apoptosis and photoreceptor cell degeneration. Neuron 28**:** 129-138.

Anderson, D. M., K. M. Anderson, C. L. Chang, C. A. Makarewich, B. R. Nelson *et al.*, 2015 A micropeptide encoded by a putative long noncoding RNA regulates muscle performance. Cell 160**:** 595-606.

Basrai, M. A., P. Hieter and J. D. Boeke, 1997 Small open reading frames: beautiful needles in the haystack. Genome Res 7**:** 768-771.

Bergendahl, L. T., L. Gerasimavicius, J. Miles, L. Macdonald, J. N. Wells *et al.*, 2019 The role of protein complexes in human genetic disease. Protein Sci 28**:** 1400-1411.

Bi, P., A. Ramirez-Martinez, H. Li, J. Cannavino, J. R. McAnally *et al.*, 2017 Control of muscle formation by the fusogenic micropeptide myomixer. Science 356**:** 323-327.

Blumenthal, T., 2004 Operons in eukaryotes. Brief Funct Genomic Proteomic 3**:** 199-211.

Bosch, J. A., N. H. Tran and I. K. Hariharan, 2015 CoinFLP: a system for efficient mosaic screening and for visualizing clonal boundaries in Drosophila. Development 142**:** 597-606.

Brand, A. H., and N. Perrimon, 1993 Targeted gene expression as a means of altering cell fates and generating dominant phenotypes. Development 118**:** 401-415.

Brent, J. R., K. M. Werner and B. D. McCabe, 2009 Drosophila larval NMJ dissection. J Vis Exp.

Calvo, S. E., K. R. Clauser and V. K. Mootha, 2016 MitoCarta2.0: an updated inventory of mammalian mitochondrial proteins. Nucleic Acids Res 44**:** D1251-1257.

Casson, S. A., P. M. Chilley, J. F. Topping, I. M. Evans, M. A. Souter *et al.*, 2002 The POLARIS gene of Arabidopsis encodes a predicted peptide required for correct root growth and leaf vascular patterning. Plant Cell 14**:** 1705-1721.

Cavener, D. R., 1987 Comparison of the consensus sequence flanking translational start sites in Drosophila and vertebrates. Nucleic Acids Res 15**:** 1353-1361.

Chacinska, A., C. M. Koehler, D. Milenkovic, T. Lithgow and N. Pfanner, 2009 Importing mitochondrial proteins: machineries and mechanisms. Cell 138**:** 628-644.

Chen, J., A. D. Brunner, J. Z. Cogan, J. K. Nunez, A. P. Fields *et al.*, 2020 Pervasive functional translation of noncanonical human open reading frames. Science 367**:** 1140-1146.

Chng, S. C., L. Ho, J. Tian and B. Reversade, 2013 ELABELA: a hormone essential for heart development signals via the apelin receptor. Dev Cell 27**:** 672-680.

Choi, H., B. Larsen, Z. Y. Lin, A. Breitkreutz, D. Mellacheruvu *et al.*, 2011 SAINT: probabilistic scoring of affinity purification-mass spectrometry data. Nat Methods 8**:** 70-73.

Chugunova, A., E. Loseva, P. Mazin, A. Mitina, T. Navalayeu *et al.*, 2019 LINC00116 codes for a mitochondrial peptide linking respiration and lipid metabolism. Proc Natl Acad Sci U S A 116**:** 4940-4945.

Clark-Adams, C. D., D. Norris, M. A. Osley, J. S. Fassler and F. Winston, 1988 Changes in histone gene dosage alter transcription in yeast. Genes Dev 2**:** 150-159.

Couso, J. P., and P. Patraquim, 2017 Classification and function of small open reading frames. Nat Rev Mol Cell Biol 18**:** 575-589.

Crosby, M. A., L. S. Gramates, G. Dos Santos, B. B. Matthews, S. E. St Pierre *et al.*, 2015 Gene Model Annotations for Drosophila melanogaster: The Rule-Benders. G3 (Bethesda) 5**:** 1737-1749.

Delanoue, R., E. Meschi, N. Agrawal, A. Mauri, Y. Tsatskis *et al.*, 2016 Drosophila insulin release is triggered by adipose Stunted ligand to brain Methuselah receptor. Science 353**:** 1553-1556.

Fricker, L. D., 2005 Neuropeptide-processing enzymes: applications for drug discovery. AAPS J 7**:** E449-455.

Galindo, M. I., J. I. Pueyo, S. Fouix, S. A. Bishop and J. P. Couso, 2007 Peptides encoded by short ORFs control development and define a new eukaryotic gene family. PLoS Biol 5**:** e106.

Golpich, M., E. Amini, Z. Mohamed, R. Azman Ali, N. Mohamed Ibrahim *et al.*, 2017 Mitochondrial Dysfunction and Biogenesis in Neurodegenerative diseases: Pathogenesis and Treatment. CNS Neurosci Ther 23**:** 5-22.

Gratz, S. J., F. P. Ukken, C. D. Rubinstein, G. Thiede, L. K. Donohue *et al.*, 2014 Highly specific and efficient CRISPR/Cas9-catalyzed homology-directed repair in Drosophila. Genetics 196**:** 961-971.

Guo, X., A. Chavez, A. Tung, Y. Chan, C. Kaas *et al.*, 2018 High-throughput creation and functional profiling of DNA sequence variant libraries using CRISPR-Cas9 in yeast. Nat Biotechnol 36**:** 540-546.

Hana, A., L. Zhen-Yuan, J. Alexandre, W. Woranontee, G. Anne-Claude *et al.*, 2020 A high-density human mitochondrial proximity interaction network. bioRxiv.

Hardie, R. C., and P. Raghu, 2001 Visual transduction in Drosophila. Nature 413**:** 186-193.

He, L., R. Binari, J. Huang, J. Falo-Sanjuan and N. Perrimon, 2019 In vivo study of gene expression with an enhanced dual-color fluorescent transcriptional timer. Elife 8.

Hoskins, R. A., J. M. Landolin, J. B. Brown, J. E. Sandler, H. Takahashi *et al.*, 2011 Genome-wide analysis of promoter architecture in Drosophila melanogaster. Genome Res 21**:** 182-192.

Hsu, P. Y., and P. N. Benfey, 2018 Small but Mighty: Functional Peptides Encoded by Small ORFs in Plants. Proteomics 18**:** e1700038.

Jaiswal, M., N. A. Haelterman, H. Sandoval, B. Xiong, T. Donti *et al.*, 2015 Impaired Mitochondrial Energy Production Causes Light-Induced Photoreceptor Degeneration Independent of Oxidative Stress. PLoS Biol 13**:** e1002197.

Kann, O., and R. Kovacs, 2007 Mitochondria and neuronal activity. Am J Physiol Cell Physiol 292**:** C641-657.

Karginov, T. A., D. P. H. Pastor, B. L. Semler and C. M. Gomez, 2017 Mammalian Polycistronic mRNAs and Disease. Trends Genet 33**:** 129-142.

Katsir, L., K. A. Davies, D. C. Bergmann and T. Laux, 2011 Peptide signaling in plant development. Curr Biol 21**:** R356-364.

Koob, S., M. Barrera, R. Anand and A. S. Reichert, 2015 The non-glycosylated isoform of MIC26 is a constituent of the mammalian MICOS complex and promotes formation of crista junctions. Biochim Biophys Acta 1853**:** 1551-1563.

Kuhlbrandt, W., 2015 Structure and function of mitochondrial membrane protein complexes. BMC Biol 13**:** 89.

Kumar, S., Y. Yoshida and M. Noda, 1993 Cloning of a cDNA which encodes a novel ubiquitin-like protein. Biochem Biophys Res Commun 195**:** 393-399.

Liu, X., K. Salokas, F. Tamene, Y. Jiu, R. G. Weldatsadik *et al.*, 2018 An AP-MS- and BioID-compatible MAC-tag enables comprehensive mapping of protein interactions and subcellular localizations. Nat Commun 9**:** 1188.

Magny, E. G., J. I. Pueyo, F. M. Pearl, M. A. Cespedes, J. E. Niven *et al.*, 2013 Conserved regulation of cardiac calcium uptake by peptides encoded in small open reading frames. Science 341**:** 1116-1120.

Makarewich, C. A., K. K. Baskin, A. Z. Munir, S. Bezprozvannaya, G. Sharma *et al.*, 2018 MOXI Is a Mitochondrial Micropeptide That Enhances Fatty Acid beta-Oxidation. Cell Rep 23**:** 3701-3709.

Nelson, B. R., C. A. Makarewich, D. M. Anderson, B. R. Winders, C. D. Troupes *et al.*, 2016 A peptide encoded by a transcript annotated as long noncoding RNA enhances SERCA activity in muscle. Science 351**:** 271-275.

Ni, J. Q., R. Zhou, B. Czech, L. P. Liu, L. Holderbaum *et al.*, 2011 A genome-scale shRNA resource for transgenic RNAi in Drosophila. Nat Methods 8**:** 405-407.

Nickless, A., J. M. Bailis and Z. You, 2017 Control of gene expression through the nonsense-mediated RNA decay pathway. Cell Biosci 7**:** 26.

Papp, B., C. Pal and L. D. Hurst, 2003 Dosage sensitivity and the evolution of gene families in yeast. Nature 424**:** 194-197.

Pauli, A., M. L. Norris, E. Valen, G. L. Chew, J. A. Gagnon *et al.*, 2014 Toddler: an embryonic signal that promotes cell movement via Apelin receptors. Science 343**:** 1248636.

Pearson, R. K., B. Anderson and J. E. Dixon, 1993 Molecular biology of the peptide hormone families. Endocrinol Metab Clin North Am 22**:** 753-774.

Pellegrino, M. W., A. M. Nargund and C. M. Haynes, 2013 Signaling the mitochondrial unfolded protein response. Biochim Biophys Acta 1833**:** 410-416.

Perkins, L. A., L. Holderbaum, R. Tao, Y. Hu, R. Sopko *et al.*, 2015 The Transgenic RNAi Project at Harvard Medical School: Resources and Validation. Genetics 201**:** 843-852.

Plaza, S., G. Menschaert and F. Payre, 2017 In Search of Lost Small Peptides. Annu Rev Cell Dev Biol 33**:** 391-416.

Port, F., H. M. Chen, T. Lee and S. L. Bullock, 2014 Optimized CRISPR/Cas tools for efficient germline and somatic genome engineering in Drosophila. Proc Natl Acad Sci U S A 111**:** E2967-2976.

Prelich, G., 2012 Gene overexpression: uses, mechanisms, and interpretation. Genetics 190**:** 841-854.

Pueyo, J. I., E. G. Magny, C. J. Sampson, U. Amin, I. R. Evans *et al.*, 2016 Hemotin, a Regulator of Phagocytosis Encoded by a Small ORF and Conserved across Metazoans. PLoS Biol 14**:** e1002395.

Richter, D. J., P. Fozouni, M. B. Eisen and N. King, 2018 Gene family innovation, conservation and loss on the animal stem lineage. Elife 7.

Saghatelian, A., and J. P. Couso, 2015 Discovery and characterization of smORF-encoded bioactive polypeptides. Nat Chem Biol 11**:** 909-916.

Sandoval, H., C. K. Yao, K. Chen, M. Jaiswal, T. Donti *et al.*, 2014 Mitochondrial fusion but not fission regulates larval growth and synaptic development through steroid hormone production. Elife 3.

Savojardo, C., N. Bruciaferri, G. Tartari, P. L. Martelli and R. Casadio, 2020 DeepMito: accurate prediction of protein sub-mitochondrial localization using convolutional neural networks. Bioinformatics 36**:** 56-64.

Snyder, S. H., and R. B. Innis, 1979 Peptide neurotransmitters. Annu Rev Biochem 48**:** 755-782.

Sopko, R., D. Huang, N. Preston, G. Chua, B. Papp *et al.*, 2006 Mapping pathways and phenotypes by systematic gene overexpression. Mol Cell 21**:** 319-330.

Stapleton, M., J. Carlson, P. Brokstein, C. Yu, M. Champe *et al.*, 2002 A Drosophila full-length cDNA resource. Genome Biol 3**:** RESEARCH0080.

Stein, C. S., P. Jadiya, X. Zhang, J. M. McLendon, G. M. Abouassaly *et al.*, 2018 Mitoregulin: A lncRNA-Encoded Microprotein that Supports Mitochondrial Supercomplexes and Respiratory Efficiency. Cell Rep 23**:** 3710-3720 e3718.

Stojanovski, D., M. Bohnert, N. Pfanner and M. van der Laan, 2012 Mechanisms of protein sorting in mitochondria. Cold Spring Harb Perspect Biol 4.

Suzuki, K., T. Hashimoto and E. Otaka, 1990 Yeast ribosomal proteins: XI. Molecular analysis of two genes encoding YL41, an extremely small and basic ribosomal protein, from Saccharomyces cerevisiae. Curr Genet 17**:** 185-190.

Szklarczyk, R., M. A. Huynen and B. Snel, 2008 Complex fate of paralogs. BMC Evol Biol 8**:** 337.

Taylor, J. S., and J. Raes, 2004 Duplication and divergence: the evolution of new genes and old ideas. Annu Rev Genet 38**:** 615-643.

Thompson, S. R., 2012 So you want to know if your message has an IRES? Wiley Interdiscip Rev RNA 3**:** 697-705.

Thul, P. J., L. Akesson, M. Wiking, D. Mahdessian, A. Geladaki *et al.*, 2017 A subcellular map of the human proteome. Science 356.

Trevisan, T., D. Pendin, A. Montagna, S. Bova, A. M. Ghelli *et al.*, 2018 Manipulation of Mitochondria Dynamics Reveals Separate Roles for Form and Function in Mitochondria Distribution. Cell Rep 23**:** 1742-1753.

Ugur, B., H. Bao, M. Stawarski, L. R. Duraine, Z. Zuo *et al.*, 2017 The Krebs Cycle Enzyme Isocitrate Dehydrogenase 3A Couples Mitochondrial Metabolism to Synaptic Transmission. Cell Rep 21**:** 3794-3806.

Usui, S., L. Yu and C. A. Yu, 1990 The small molecular mass ubiquinone-binding protein (QPc-9.5 kDa) in mitochondrial ubiquinol-cytochrome c reductase: isolation, ubiquinone-binding domain, and immunoinhibition. Biochemistry 29**:** 4618-4626.

Van Der Kelen, K., R. Beyaert, D. Inze and L. De Veylder, 2009 Translational control of eukaryotic gene expression. Crit Rev Biochem Mol Biol 44**:** 143-168.

Veitia, R. A., S. Bottani and J. A. Birchler, 2008 Cellular reactions to gene dosage imbalance: genomic, transcriptomic and proteomic effects. Trends Genet 24**:** 390-397.

Verstreken, P., C. V. Ly, K. J. Venken, T. W. Koh, Y. Zhou *et al.*, 2005 Synaptic mitochondria are critical for mobilization of reserve pool vesicles at Drosophila neuromuscular junctions. Neuron 47**:** 365-378.

Viswanatha, R., Z. Li, Y. Hu and N. Perrimon, 2018 Pooled genome-wide CRISPR screening for basal and context-specific fitness gene essentiality in Drosophila cells. Elife 7.

Wang, J. W., E. S. Beck and B. D. McCabe, 2012 A modular toolset for recombination transgenesis and neurogenetic analysis of Drosophila. PLoS One 7**:** e42102.

Wu, C. F., and F. Wong, 1977 Frequency characteristics in the visual system of Drosophila: genetic dissection of electroretinogram components. J Gen Physiol 69**:** 705-724.

Xue, Z., M. Ren, M. Wu, J. Dai, Y. S. Rong *et al.*, 2014 Efficient gene knock-out and knock-in with transgenic Cas9 in Drosophila. G3 (Bethesda) 4**:** 925-929.

Yanagawa, S., J. S. Lee and A. Ishimoto, 1998 Identification and characterization of a novel line of Drosophila Schneider S2 cells that respond to wingless signaling. J Biol Chem 273**:** 32353-32359.

Yang, L., and A. Veraksa, 2017 Single-Step Affinity Purification of ERK Signaling Complexes Using the Streptavidin-Binding Peptide (SBP) Tag. Methods Mol Biol 1487**:** 113-126.

1600 Yeasmin, F., T. Yada and N. Akimitsu, 2018 Micropeptides Encoded in Transcripts
1601 Previously Identified as Long Noncoding RNAs: A New Chapter in
1602 Transcriptomics and Proteomics. Front Genet 9**:** 144.
1603 Yosten, G. L., R. M. Lyu, A. J. Hsueh, O. Avsian-Kretchmer, J. K. Chang *et al.*, 2013 A
1604 novel reproductive peptide, phoenixin. J Neuroendocrinol 25**:** 206-215.
1605 Zhang, S., B. Reljic, C. Liang, B. Kerouanton, J. C. Francisco *et al.*, 2020 Mitochondrial
1606 peptide BRAWNIN is essential for vertebrate respiratory complex III
1607 assembly. Nat Commun 11**:** 1312.
1608 Zhou, R., I. Hotta, A. M. Denli, P. Hong, N. Perrimon *et al.*, 2008 Comparative analysis
1609 of argonaute-dependent small RNA pathways in Drosophila. Mol Cell 32**:** 592-
1610 599.
1611

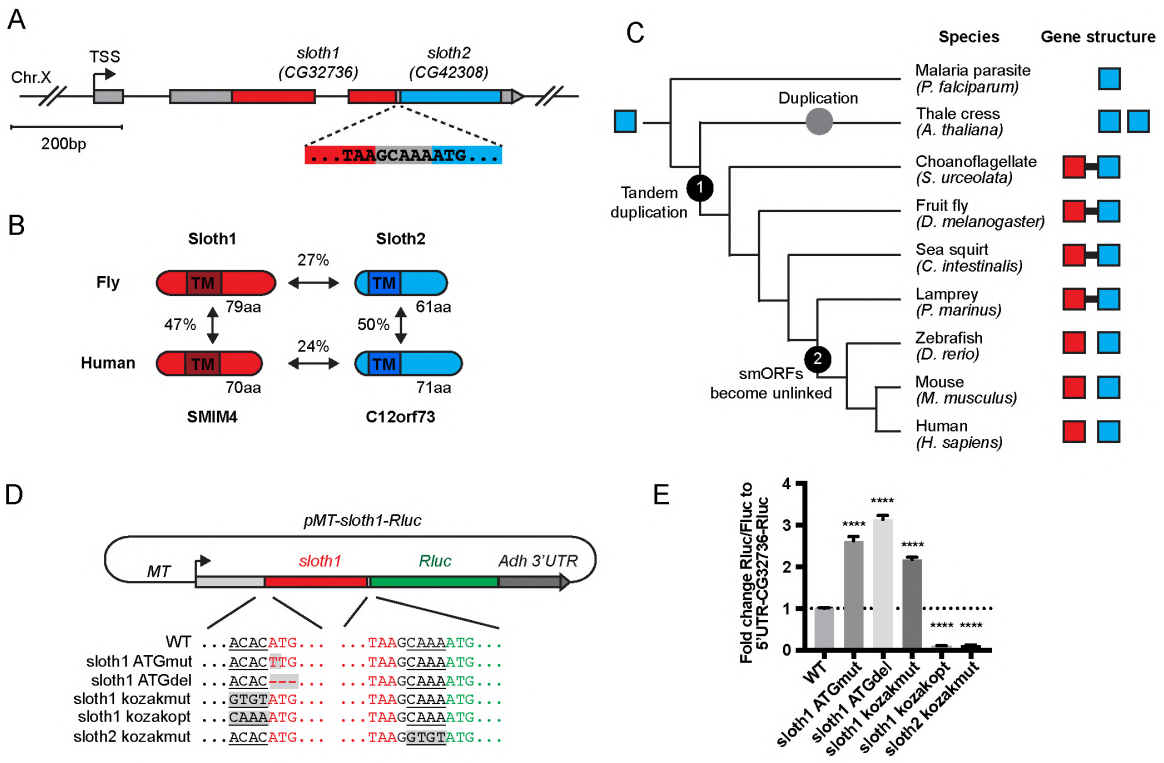

Figure 1

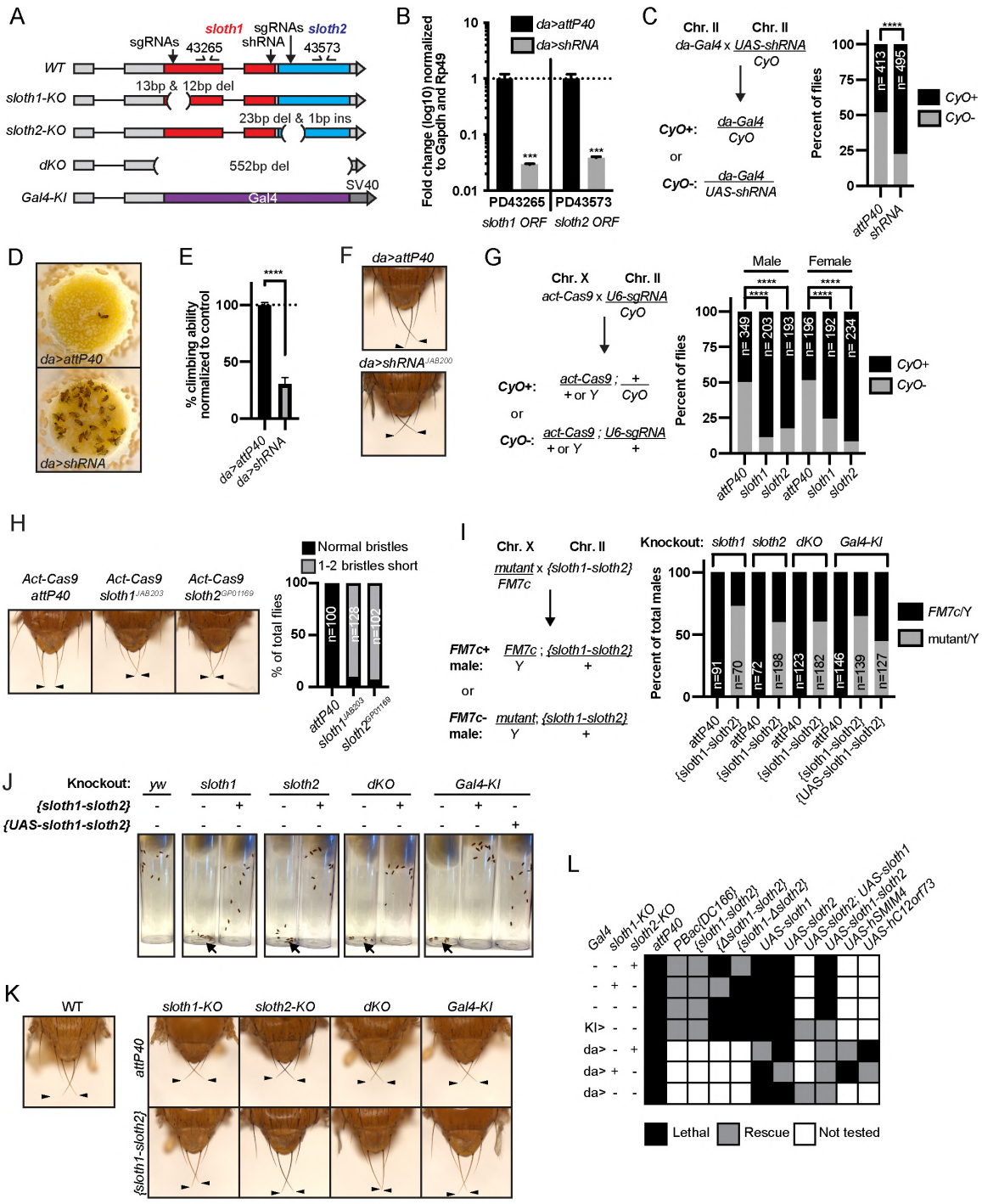

Figure 2

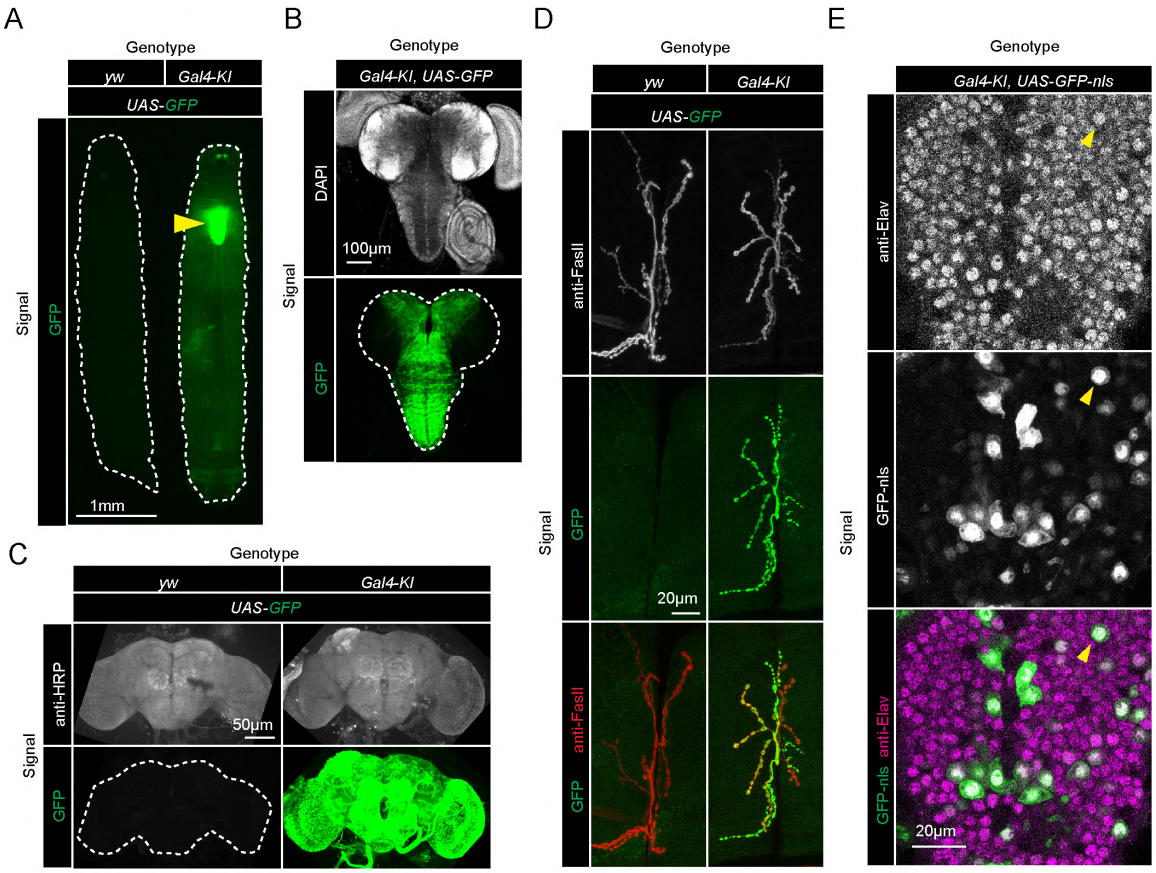

Figure 3

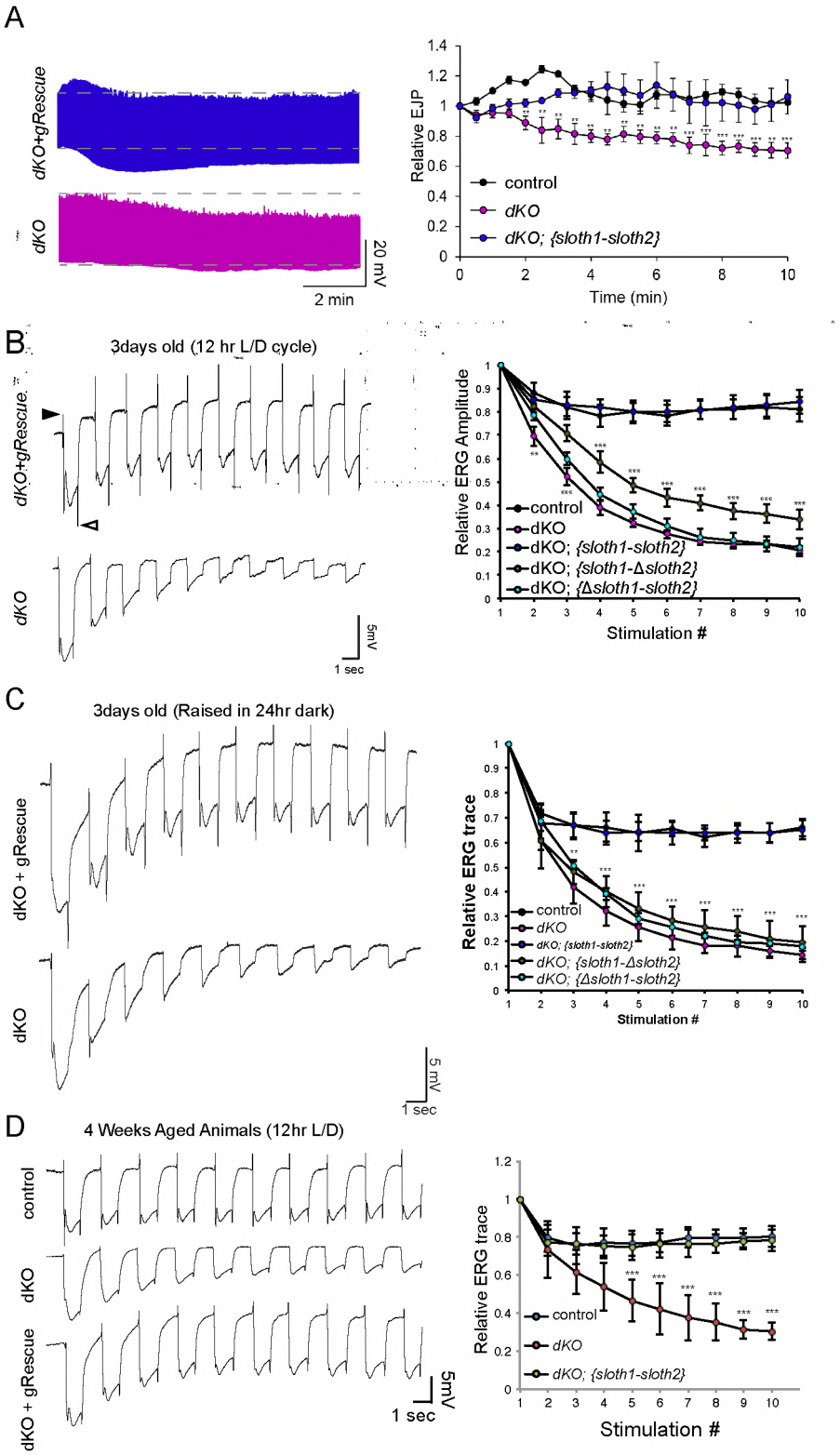

Figure 4

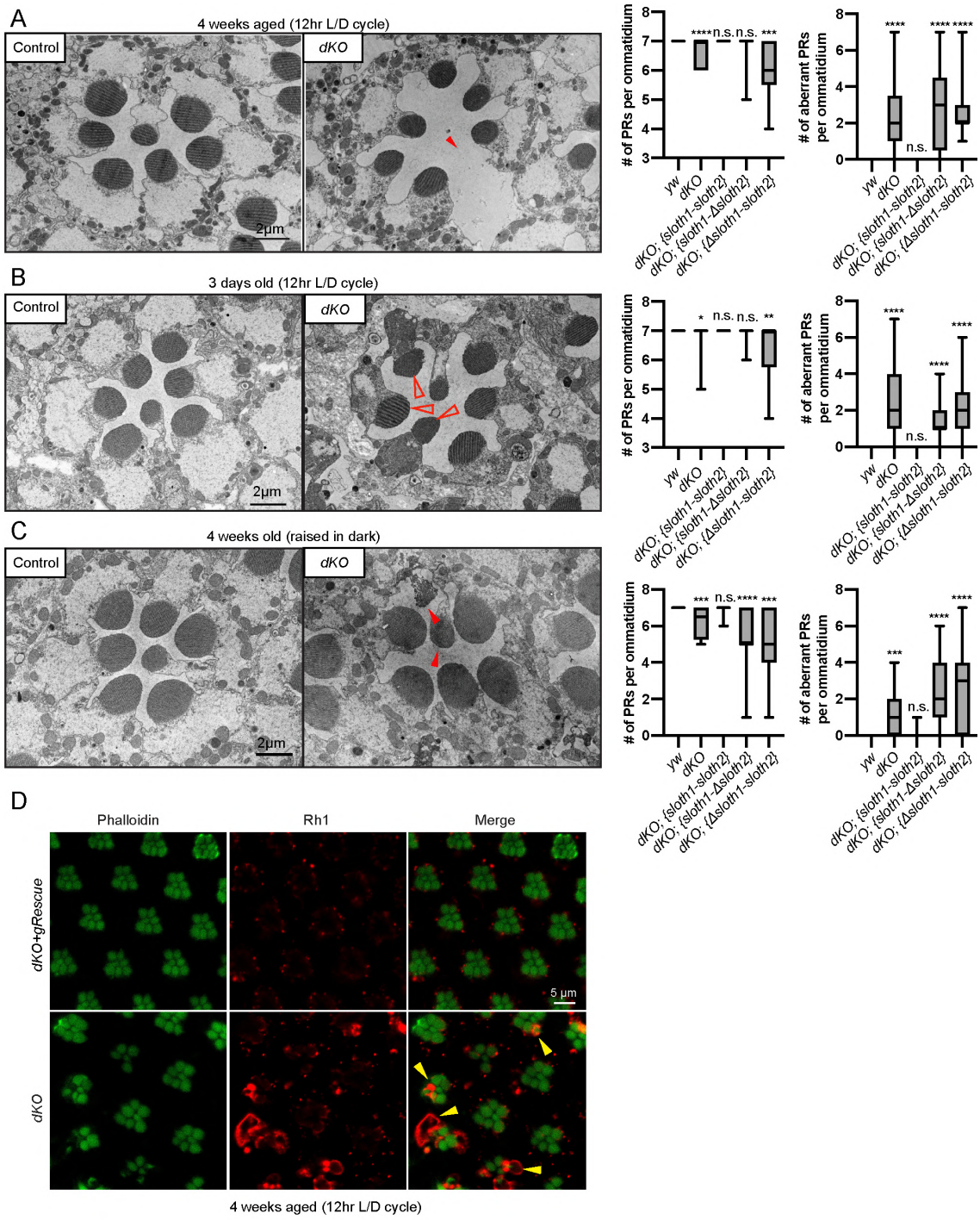

Figure 5

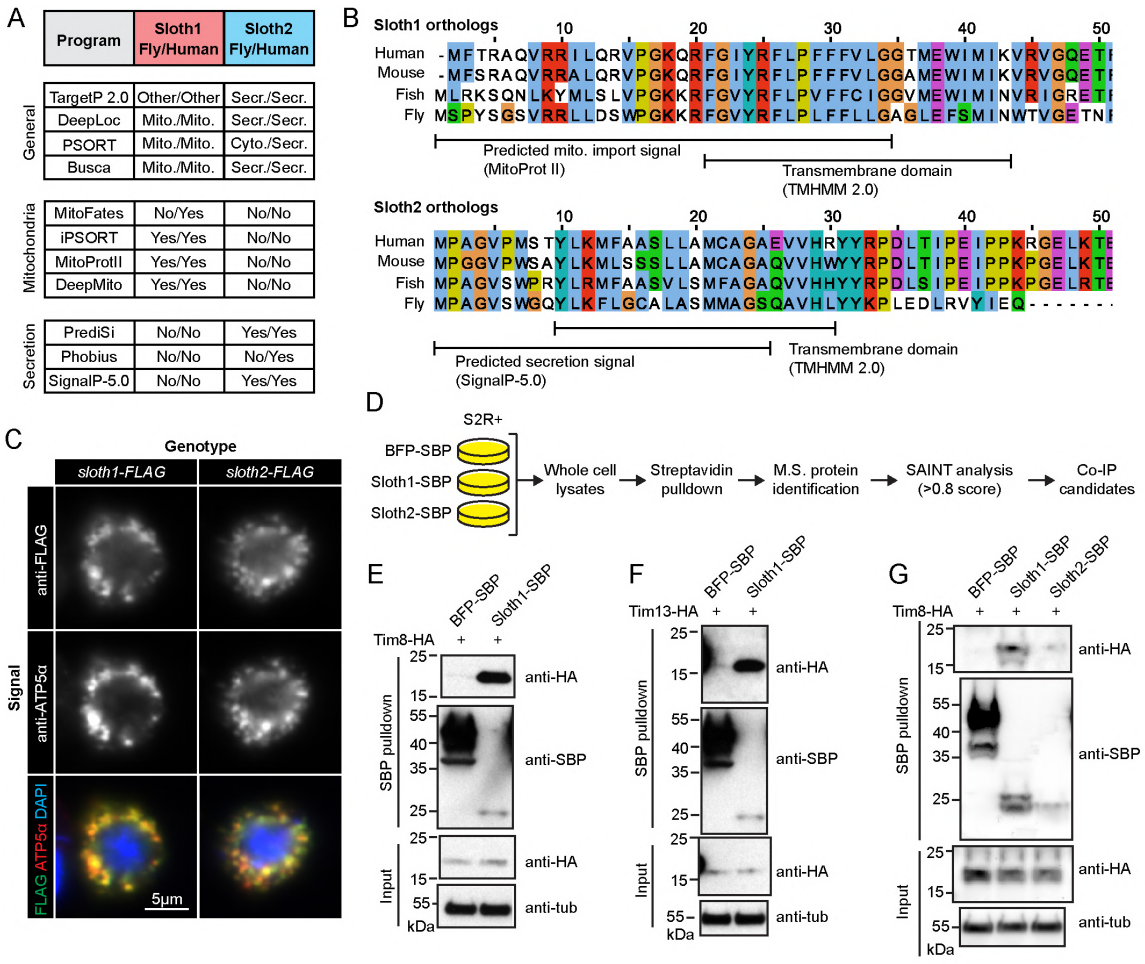

Figure 6

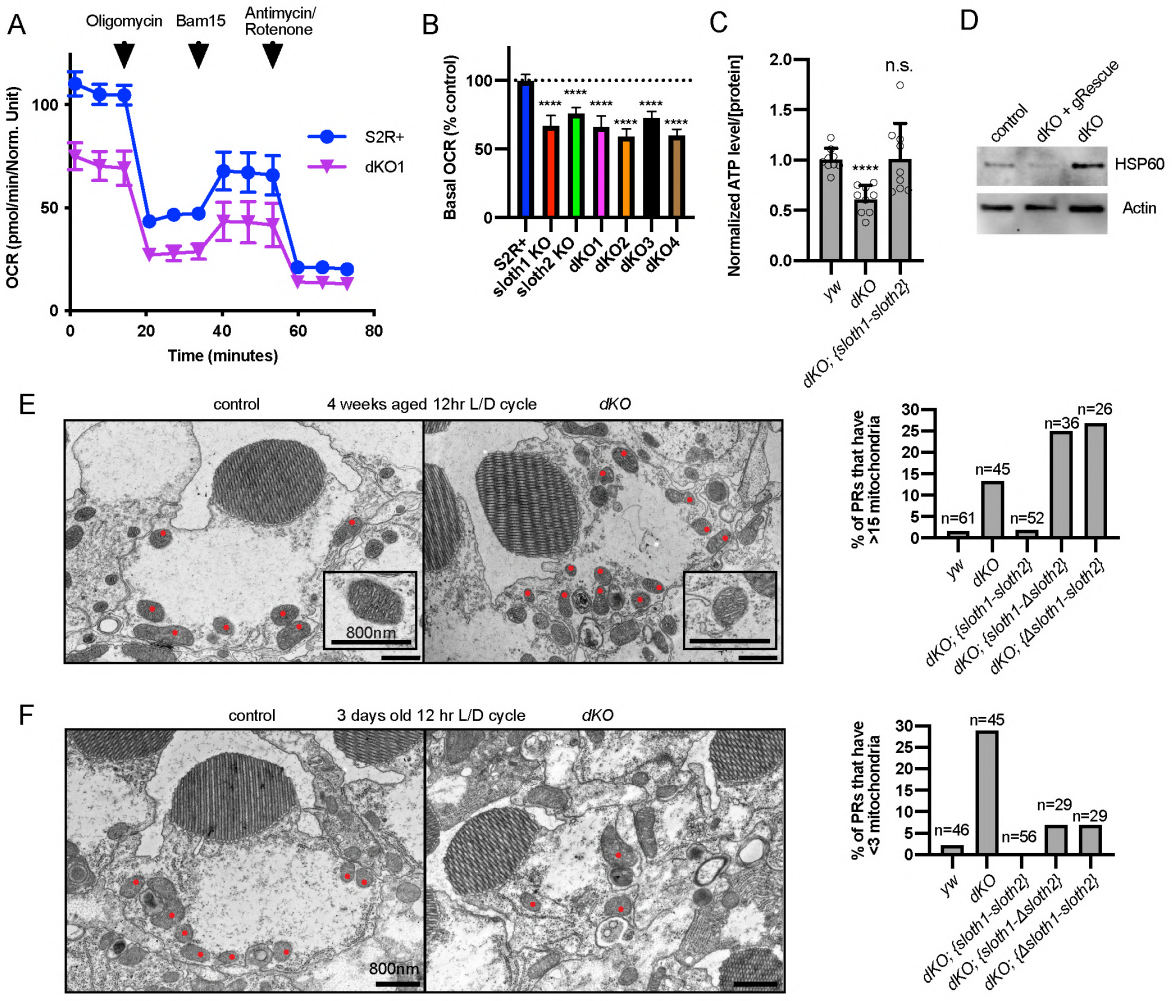

Figure 7

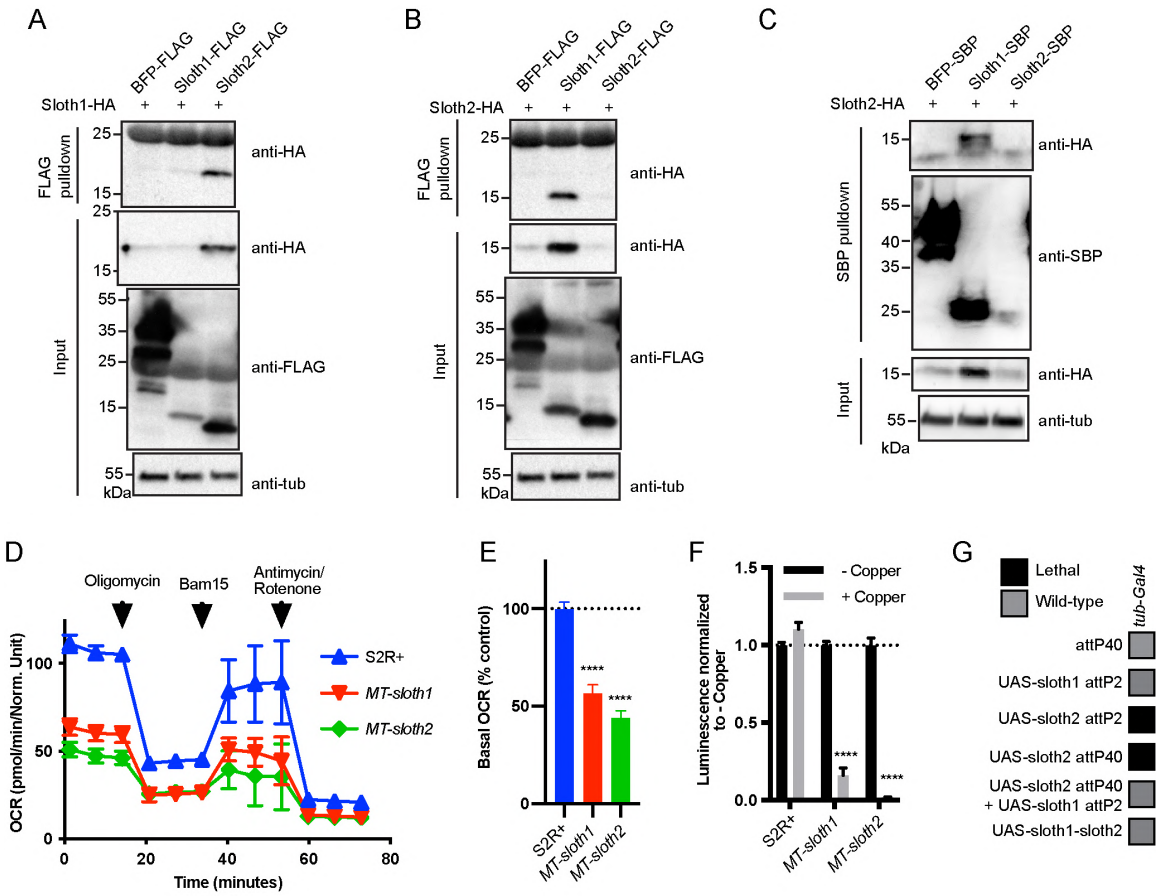

Figure 8

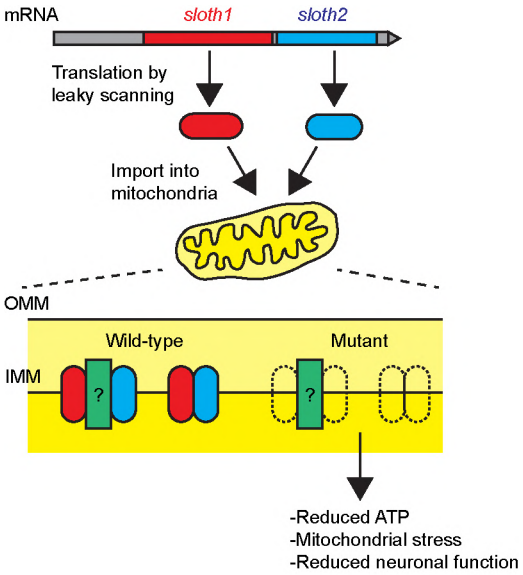

Figure 9 or Graphical abstract

Supplemental Figure 1

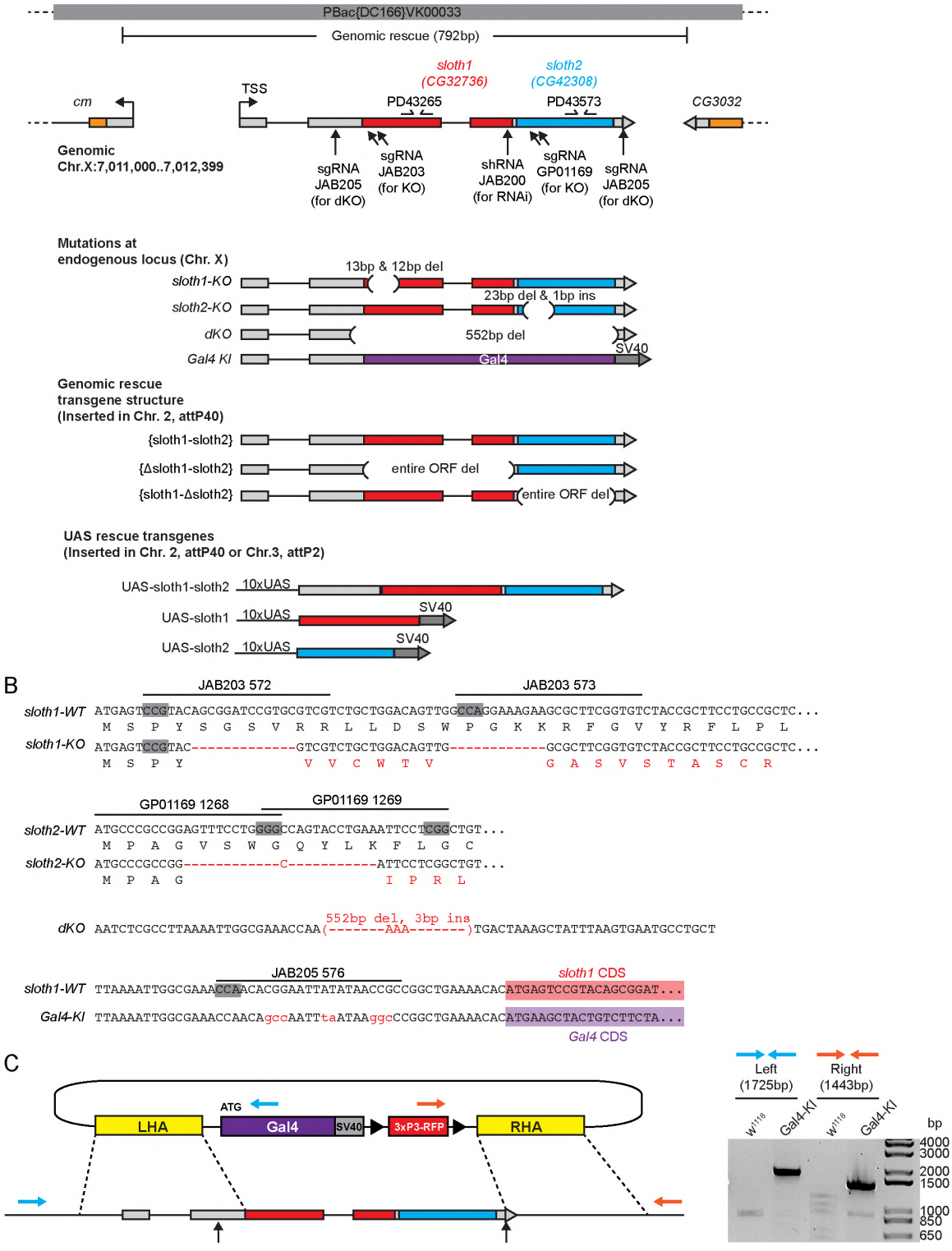

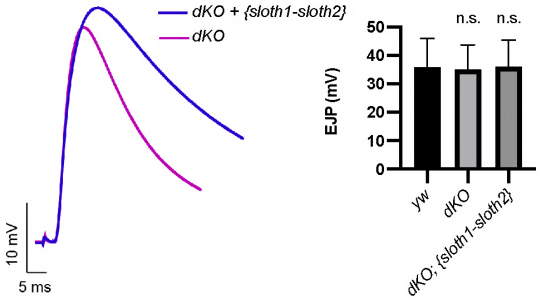

Supplemental Figure 2

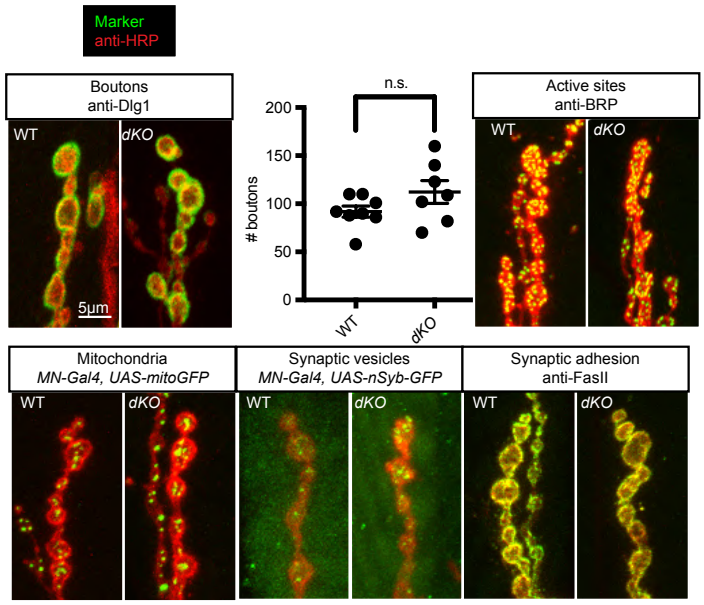

Supplemental Figure 3

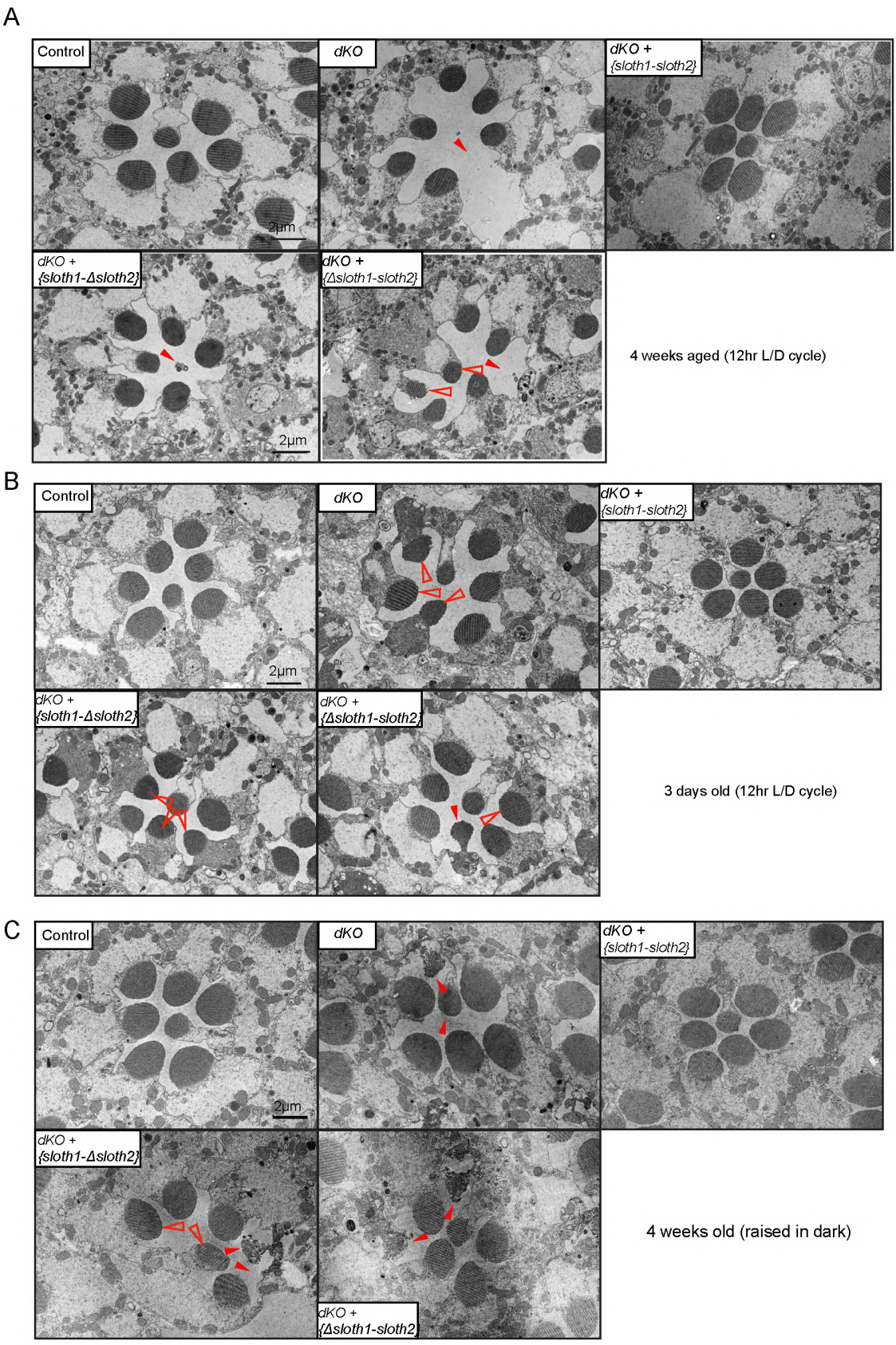

Supplemental Figure 4

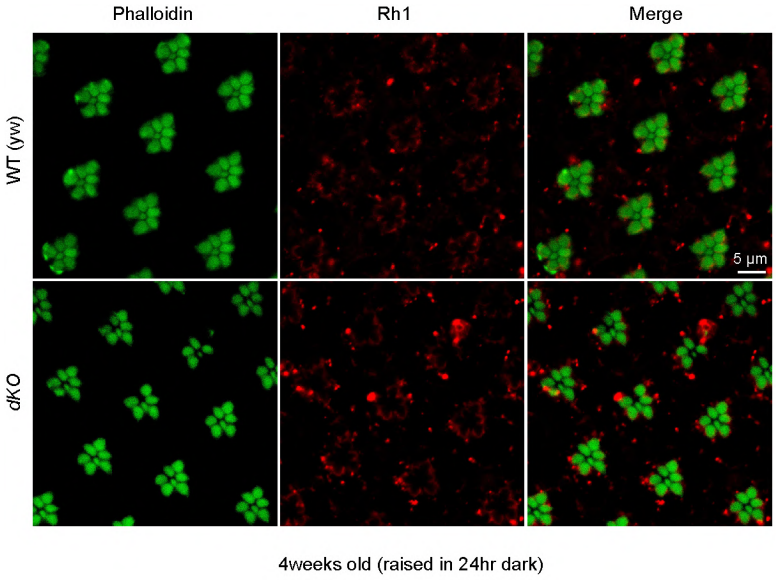

Supplemental Figure 5

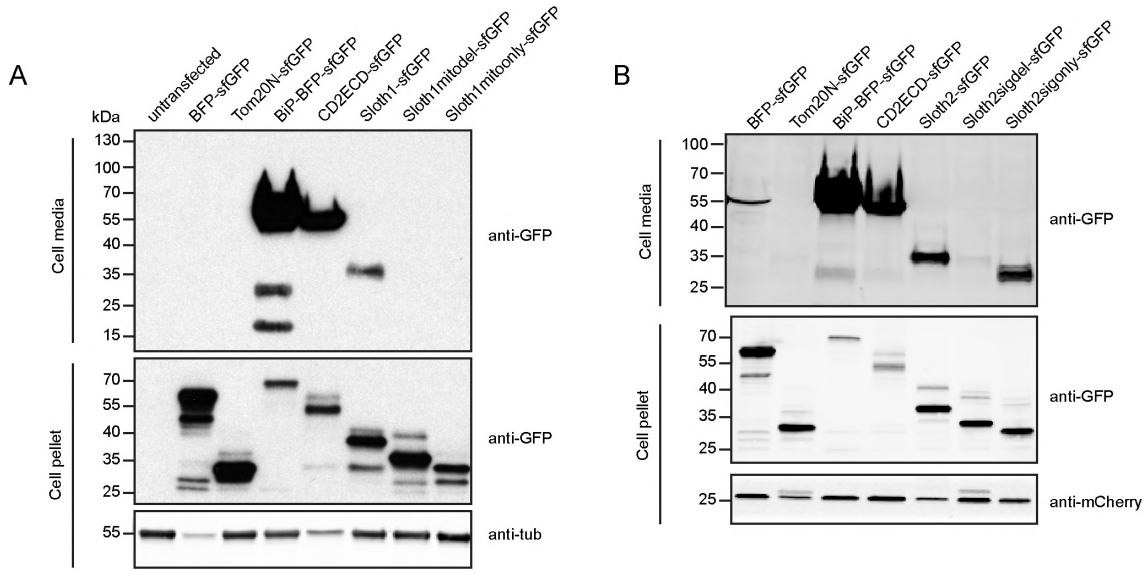

Supplemental Figure 6

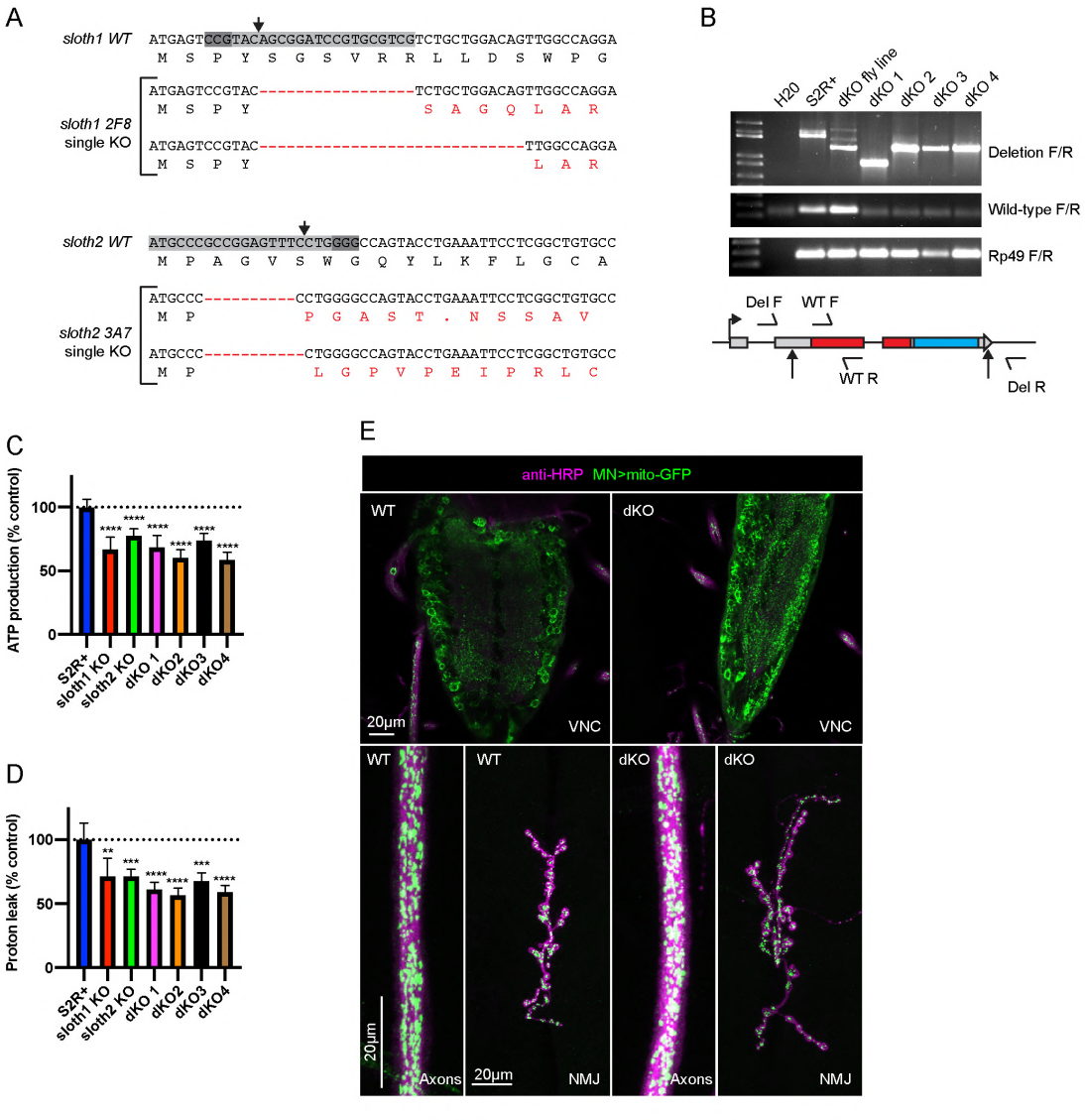

Supplemental Figure 7

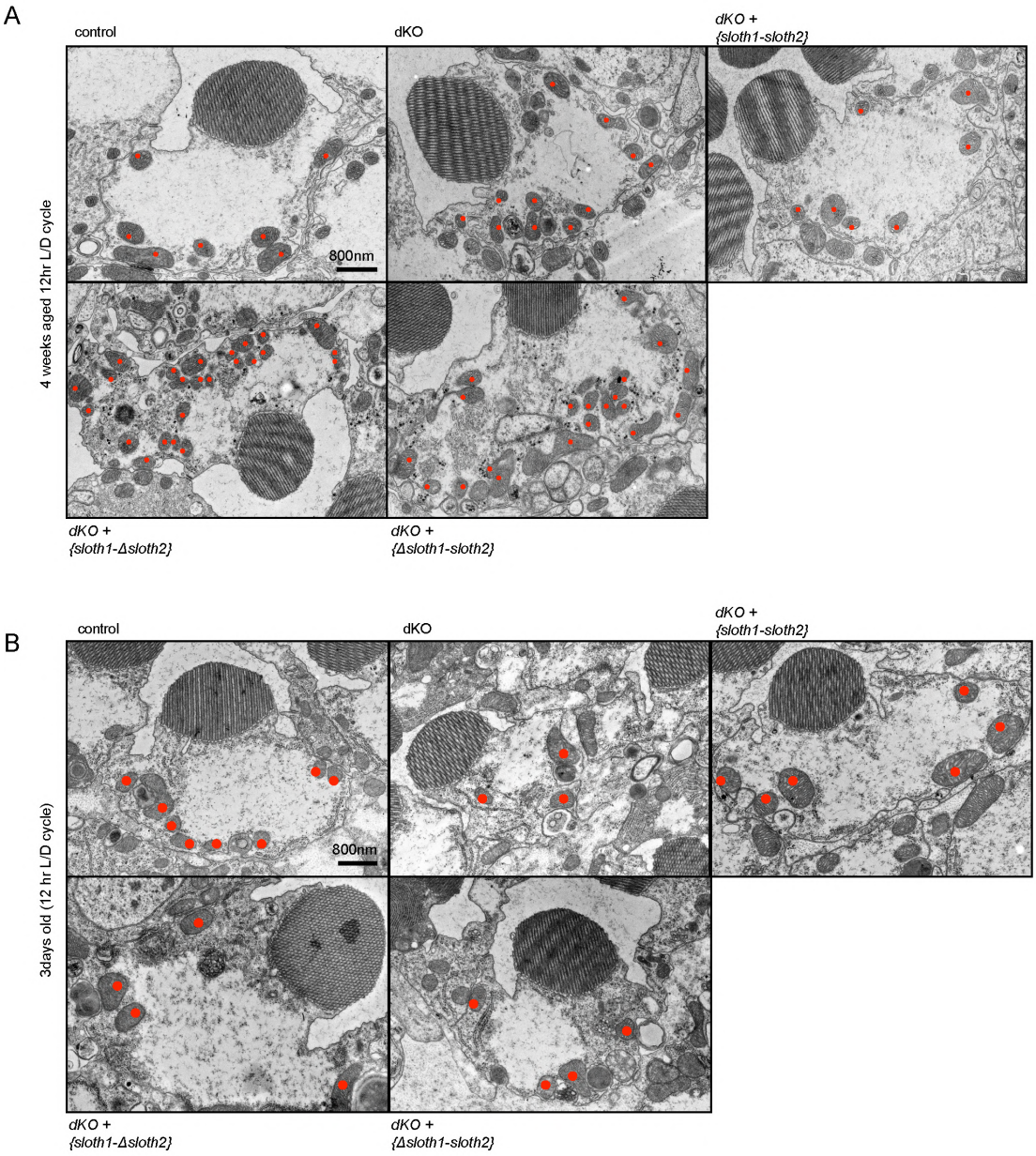

Supplemental Figure 8

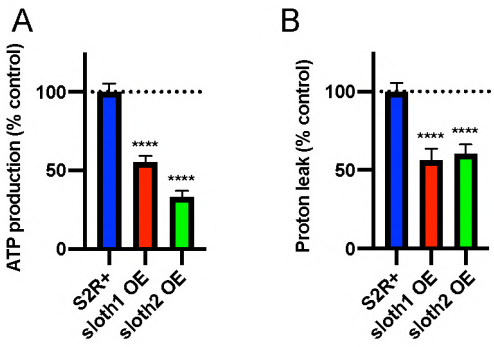

Supplemental Figure 9

Supplemental File 1

Genomic sequences of *sloth1* and *sloth2* homologs

BOLD = Coding sequence
Red = *sloth1* homolog
Blue = *sloth2* homolog
Underline = Coding sequence overlap

>Dmel_sloth1-sloth2(CG32736-CG42308)
AATCGAACAGCTGATTGCTGCGAACCGGAACAAATGGAAATTGTATCGTGAGgcaagtg
gagtttccctttacttttggCAAATAATAAATAAACAAAGGAACAAGCCTAAACATTT
TCAATTAAACCATATACAGAACTAACGCACACATGTGACGGAGGCAATACACAAACACG
GCACCTTTGAATCTCGCCTTAAAATTGGCGAAACCAACACGGAATTATATAACCGCCGG
CTGAAAACAC**ATGAGTCCGTACAGCGGATCCGTGCGTCGTCTGCTGGACAGTTGGCCAG**
GAAAGAAGCGCTTCGGTGTCTACCGCTTCCTGCCGCTCTTCTTTTTACTGGGCGCCGGC
CTGGAATTCTCCATGATCAATTGGACAGTGGGCGAGACCAATTTCTgtgagactgctac
gcttaaaaccttacttttatttactaatacggaatcttttccatgcag**ACCGCACTTTT**
AAGCGCCGCCAGGCGAAGAACTACGTGGAAGAGCAGCAGCATCTGCAGGCGCGAGCCGC
GAATAACACCAACTAAGCAAA**ATGCCCGCCGGAGTTTCCTGGGGCCAGTACCTGAAATT**
CCTCGGCTGTGCCCTGGCATCCATGATGGCCGGATCGCAGGCTGTTCACCTTTACTATA
AGCCTCTGGAGGACTTGCGCGTCTACATCGAACAGGAGCAACACAGCACACAGGTGGAT
CCCACCGCAAAGCCACCGGAATCTGCATAACACTGTGTACTAGACAAGTTATTGGTGAC
TAAAGCTATTTAAG

>Choanoflagellate_Salpingoeca_urceolata_sloth1-
sloth2_comp15074_c0_seq2
TTCACTTTCGTTTTCTTACTGTTTCAACGTTGCGACTGTGCTCTTCGGCTTCACGTGTT
CTTGCACCATCTGCTGTGGCACCCATTCAGCGCAGAGTTCAGCGGTCCACGCAGTGGCA
GCGGGCCAGGACACCACTTCTGCTTGGGTACCTCTA**ATGCCGCGTTCGTTTCCGCAAAT**
TGCGGCGCGTGTGGTGCCTGTGTCGTTTGCTCTTGGCGCGTTTATGGAATGGTTCATGC
TCAACGTTCAAATTGGCCACGAAACCTTTTATGACACTGCAGTGAGGCTGGAAGCAAAG
CGACGGTTTGAACAACAGCAAGAGGAGCAGCAAAAAGCTAGCAACGACCCTTCGTCCGA
CTCACCGCCGCCAGCAGCATCCTAAGAGTTGTTTGCTTCCTGAAGTAGTTTTAGTTTGT
ACCTGTTGTTTTTCGTTAGTTTTTTTGAAGGTTCCTTCACGTCCAGCACC**ATGCCGTTT**
GGTGTTTCCATGTCTCGGTACGTGGGTGTGGTCGCACTTACCCTCGGGTCCATGCTGGC
CGGTGCTTCCACCGTACACTACTTCTACCAGCCCGACCTGACTGTGCCCACCGAGCCTC
CTCCGGCGCCGGATTCCGTGTTGAAAAAGCCACGGATAGCCTTGGTGTCGCCACGGCAG
CGTGCGACGGGAGAAGCAGACGATGGAAAACAGTGACCGGTCTTATGCGTGATTGGTAT
TAAACACATGGTCGTGTTCAAGATGAGGTTGTTGGTTGCCAGTGCCGCGGAAAACCCGC
AACATGGGCGCTTGTCCCAATACGTTTTTGCTGTGGGGTGTTCGTTTTTCTTTTTCCGG
TTGGTTGTTTCATCCTCATTCGCCACGCAGCAGCAAAAAGCAACAAGTCAACTCGATTG

>Lamprey-Petromyzon_marinus_sloth1-sloth2
TTTCTGTCTGTGCCCGCGTGTCTCTGTGTCCACATGTCTGTCTGTCCATGTGTCAGGGG
GTGCAGCGGGCGAATGGGCG**ATGGTGTTCTTCAGCAGCGCTCTCGGGAGGATTCTCAGT**
AAAGTTCCCGGAGAGAAGAGGCTGGGTGTCTATCGGTTCCTGCCCGTGTTCTTCGTGAT
TGGCGGTGCCATGGAGTGGATCATGATTAACATGAGAGTCGGCAGAGAGACCTTCTGTG

GGTACCACGCAGGGCTTCATTATTTCTCACTGAAATATTTTCCGGGTGACCGGTAGACT
GGAGTTGGTTGCACATGATTAGTATCCACGGCCTGGTAGCCCTGAACAGCGCCTACACT
GGAATCGGGACTCGCATGCCACGCGTTTGACTCTTCGTTTGACCCTTCGTTTGACCCCG
GCGTCCCATTATTTACCTCTGACACCGCATGCTCACCATCGAGTGCGACTAACCGCACG
CGACGGCGCGCTGTTTCTTTCAG**ACGACGTCTACAGACGCAAGCAGTCGGAGCGCCGTT**
ACCAGCAGCGCCTCGCCGAGACCTCGCAGTCCAGCGGTTCCAACTAAGAGTCTCGCCTT
TCTCGAACAGACGATCGACTCGGTCACCACCCCACACGTCACTCCGTCTCCTCCCCCCC
TTCCCGCCGTTGTTGCTGCCGCCGCTGCCACCACAACCGACTTGCGCTGCTTGCGTAGA
AGCTACGGGCGCAAAGAACTGACGGCTCGCACTGGGCCGTGCGTGAGACTTTCGGAGCG
AGGTTGTTGACA**ATGCCGGCGGGCGTGACGTGGCCGCGCTATCTCAAGATGCTGACCGC**
GAGTCTCCTGTCAATGCTGGCAGGAGCGGAGGTGGTTCACCGCTACTACCGGCCAGACC
TGGTACGTGGACTTTTTTTCTTTCGTTCTCAGGAGTCCGGCTCGGGGATATAAAATGTT
CACGTTATAAGCCATTTCATTGAGCTATCATATGTGATAACCAGGTCGCTTCTGAAAAA
GAGCTAAATTACTCATTGGGCCTTACCTAGTAAAAAAAAATCCCACTGAGTGTTTTCCG
GGTCTCTGGTTAAACCCAAGAAGGTGACTCGCAGTAGCCGCAACCATAGCGAAGGAGGT
ATACTTGATGTGGTGTGTTGGGTGCAGAAATACAGGACCCCAAGAGACGCTGCTACCCG
TAGTGTATCTGTGTGGATATCCGGTGTTAATTGCCATGTAAGAGTGGGTAAGAGGATAT
TTCGATAGTACCACCCCAACAGGGATAAAGAGGGGTTTCCACCGCATTGCTGTTGTTCA
CTGTTGCGGTTTCCCTCCCACACAG**AGCATCCCTGAGGTTCCGCCAGCGCCGGGGCAAC**
TGCAGACGCGGCTGTTGGGCATCGAGGGCACAACGGGGACACCACTCAGTGGCACCAGG
GCTGCGGAGGAGGAACGCAGCCATCCCTCGTGACGGCGTCCACTCCCTCAACCTCGAGC
ACGTGCACGTGCACGAGTTAACGCACACACGAACATGCACAGGAGGCACAGCACATGCA
CAGAATGTTATACCTCCTTCACGATGGTGAATCAAAAACGATAAGACTTTTTATTTTAC

>seasquirt_XM_018812254.2_sloth1-sloth2
TTCAAAACAGAACAGTTATCAAATGTATTATGTAAAAATGCAGTTGAGTATATGAGTAA
GCCAGTAGTACATAATATAAACCATACCCTCGGTCTGGAGCCACAAATACTTAAAACAA
ATACGGCTAATACTTTTTGTAATATTCTAGTAACAAAACCTGATTTTTAAACATATTTG
GCCCATTTTAGAGTTGTAAAGTATGAATTGTTTCTAGT**ATGACGTTTATTGGTCGACTG**
GTCCAGACATTTCTTTACTACTACCCAATAAAAAGACAAAGCCCATACAAATTCGTTCC
ACTGTTTTTTGCCATTGGAGCGTCTGTGGAGTGGGTTATGATAAAAGTTCCGGCTGCAG
GACGAGGTGAAACATTTTACGACGTTTGGAGAAGAAATAGATCAGAAAAAGAATACAAG
CAGAGAATAATTGAAGAGAAATTTCAAGAAGCAATTAAAGCAAAAGAAAACTGTGAAAA
TTAATAAGCATATATTTGGCTTGTCTTAAACTGCATTAAACACTTAATTTAAATAAATT
ACCTTTGAAAAAATCAATAATTTACTTTTATTATAAGTTTAAACAGTTTTTTTAGCTTG
AACTTGCGTAAAGAAATTTAGGCCTAAAATTAAAAATCACCCAAAAACACTTTCTGTTC
ATTTAATAAGCAAAACCTTTTGTTTGATTTATTTTCCAACTGTATAATTTTGCATACCC
ACCACATC**ATGCCTTATGGTGTTTCTTGGCCATTCTACCTGAAAACAGTATCTTCTTCA**
CTCATAGCAATGTTCCTGGGCTCACACAGTGTTCATATGTGGTACAGACCTGATCTATC
CATACCTGAGATCCCACCTAAAAAAGGGGAGCTTCACACAAAACTTTATACAACAAAAT
CAGAAAATTAAACGAATTCATTACTTTTGTTAATGTTTTTTTGGTAACCTTAATCCAGT
GTGCAGTTGTACTATACGCTTATTTTTTTTTTGGTAGCTTTGTTTCAGCTAGTTACTTG
TTTTCTATCAGGTATACTGGTAATGTTTTGGTTTACATTTATTTATGAAGAAGATAAGT
TTCCTTCTGCTAAGTAAAAGTTGGCATTTTAAATGTAATTCACTTTAAAAACCCATATT
TCAGTTTCATTTCATAACGCTTTTTGTGTTTGATCAATTTTTGGCTGTGAACAAATTTT
GTGTTTGTTTGACTCAACCTAAAAACATCTCCTTACTTATTAGGTTGACTGTATAGGGC
AAAGTAGTTTTCAAACATTGTATAACTTTTCAAGATGGCCGACAACCTTAGTGAAGAAT
GGTGGCAAACGGCAGTTTCTGATGAAGAAGAAGGCGCAAGTGATGATGGTGAACGAAAA

GAAATGAAACGTAAACTGAACGAACCGACTTCAGGAATAGTAGTTTCAGAAAACGAGGA
ACCAGAAGTGAAAAAGAAAAAAAGGCGGAACAGAAAAAGAATTACTGAAGCTAAGCTTC
CCGATCAAGGGGATTCACCCACGATGTTACGAGATTATCTCAAACTTCACTTCAGTAAA
TTATCCAAGCTCGAATTTGAGGATATTTCGCTAACAGAATCCAATTTCACAGCATGCAA
TATCGACAAAGAACATACTACCACGTCGTATTTTAAACAAATCGCCCCCAAGTGGCATC
GTTTAAGCACAGCTCACAGTCACAAGATGTCGCCTCTGATCATCGTGGTTTGTGGCAAC
GCACTTCGAGCGTCGAAATTTAACACAGAAGCAAAGACTTTTAAGGGCAAAGATGCAAG
GTCGATAAAGCTATTTGCGCGCCACATGAAGATCGACGATCAAATCAAACTTCTGCGGG
AAAACGTCATTCATTTCGCCGTCGGCACACCGGAAAGAATCCGATCTCTTATCCTACAA
GATGCTCTCAGTTTAGAACACACTCGAGCGTTTGTCATCGATTGGAATTGGAGAGATGT
AAAACTAAAGCGTTTAATTGACATACGAGAGGCTCGTGCGTCGTTGATGAATTTGTTAA
AAGATTGCGTGATCCCAGCTTGTAAGAAACACCATGTAAAAATCGGGTTGTTTTGATTT
GAATTTGTGCAAAAAATGAGGTTTTCTGACGTCATACAGGTTCAAAATTTGCTTGTGTG
CATGGCCCGTTTTTTTCAGTAAATGGTTTACGTTCATGCAATAAATTGCCATTTTAAGT
TAGTGTA

Supplemental File 2

Name	Sequence	Description
JB749_MT-Rluc_backboneF	ATGACTTCGAAAGTTTATGATC	Cloning pMT-sloth1-Rluc
JB750_MT-Rluc_backboneR	GAATTCCCCTTTAGTTGCAC	Cloning pMT-sloth1-RLuc
JB751_CG3242_5'UTR_overlapMTRluc_F	gtgcaactaaaggggaattcAATCGAACAGCTGATTGC	Cloning pMT-sloth1-RLuc
JB752_CG3242_5'UTR_overlapMTRluc_R	tcataaactttcgaagtcatTTTGCTTAGTTGGTGTTATTC	Cloning pMT-sloth1-RLuc
JB753_CG32_SDM_ATG_TTG_F	ctgaaaacacTTGAGTCCGTACAGCGGATC	Cloning pMT-sloth1-RLuc derivatives by SDM
JB754_CG32_SDM_ATG_TTG_R	acggactcaaGTGTTTTCAGCCGGCGGTTATATAATTC	Cloning pMT-sloth1-RLuc derivatives by SDM
JB755_CG32_SDM_ATG_del_F	ctgaaaacacAGTCCGTACAGCGGATC	Cloning pMT-sloth1-RLuc derivatives by SDM
JB756_CG32_SDM_ATG_del_R	acggactGTGTTTTCAGCCGGCGGTTATATAATTC	Cloning pMT-sloth1-RLuc derivatives by SDM
JB757_CD32_SDM_kozak_GTGT_F	ctgaaagtgtATGAGTCCGTACAGCGGATC	Cloning pMT-sloth1-RLuc derivatives by SDM
JB758_CD32_SDM_kozak_GTGT_R	acggactcatACACTTTCAGCCGGCGGTTATATAATTC	Cloning pMT-sloth1-RLuc derivatives by SDM
JB759_CD32_SDM_kozak_CAAA_F	ctgaaacaaaATGAGTCCGTACAGCGGATC	Cloning pMT-sloth1-RLuc derivatives by SDM
JB760_CD32_SDM_kozak_CAAA_R	acggactcatTTTGTTTCAGCCGGCGGTTATATAATTC	Cloning pMT-sloth1-RLuc derivatives by SDM
JB773_CG42_SDM_kozak_GTGT_F	accaactaagGTGTATGACTTCGAAAGTTTATGATCCAG	Cloning pMT-sloth1-RLuc derivatives by SDM
JB774_CG42_SDM_kozak_GTGT_R	tcgaagtcatACACCTTAGTTGGTGTTATTCGC	Cloning pMT-sloth1-RLuc derivatives by SDM
JB567_CG32736_shRNA3_top	ctagcagtGCCGCGAATAACACCAACTAAtagttatattcaagcatataTTAGTTGGTGTTATTCGCGGCgcg	Oligos annealed and ligated into pValium20 for shRNA expression
JB568_CG32736_shRNA3_bot	aattcgcGCCGCGAATAACACCAACTAAtatgcttgaatataactaTTAGTTGGTGTTATTCGCGGCactg	Oligos annealed and ligated into pValium20 for shRNA expression
JB572_CG32736gRNAdKO_F	TATATAGGAAAGATATCCGGGTGAACTTCgCGACGCACGGATCCGCTGTAGTTTTAGAGCTAGAAATAGCAAG	to construct pCFD4-sloth1 (aka JAB203)
JB573_CG32736gRNAdKO_R	ATTTTAACTTGCTATTTCTAGCTCTAAAACGGAAAGAAGCGCTTCGGTGTcGACGTTAAATTGAAAATAGGTC	to construct pCFD4-sloth1 (aka JAB203)
GP01169_F	TATATAGGAAAGATATCCGGGTGAACTTCGATGCCCGCCGGAGTTTCCTGGTTTTAGAGCTAGAAATAGCAAG	to construct pCFD4-sloth2 (aka GP01169)
GP01169_R	ATTTTAACTTGCTATTTCTAGCTCTAAAACAGGAATTTCAGGTACTGGCCGACGTTAAATTGAAAATAGGTC	to construct pCFD4-sloth2 (aka GP01169)
JB576_CG32736_CG42308gRNAdel1_F	TATATAGGAAAGATATCCGGGTGAACTTCGCGGTTATATAATTCCGTGTGTTTTAGAGCTAGAAATAGCAAG	to construct pCFD4-sloth1-sloth2 (aka JAB205, for dKO)
JB577_CG32736_CG42308gRNAdel1_R	ATTTTAACTTGCTATTTCTAGCTCTAAAACATAACTTGTCTAGTACACAGcGACGTTAAATTGAAAATAGGTC	to construct pCFD4-sloth1-sloth2 (aka JAB205, for dKO)
JB628_CG32-42_LH_EcoRI_F	cccttcgctgaagcaggtggGCCTCGTTGTTGGTGTAC	to amplify LHA
JB634_CG32-42_LH_Gal4SV40_R	gtagcttcatggtgTGTTGGTTTCGCCAATTTTAAG	to amplify LHA
JB635_CG32-42_Gal4SV40_LH_F	gaaaccaacacaccATGAAGCTACTGTCTTCTATC	to amplify Gal4-SV40
JB636_CG32-42_Gal4SV40_loxP_R	acgaagttatAGACATGATAAGATACATTGATG	to amplify Gal4-SV40
JB637_CG32-42_loxP_Gal4SV40_F	tatcatgtctATAACTTCGTATAATGTATGCTATAC	to amplify loxP-RFP-loxP
JB631_CG32-42_loxP_RH_R	gtcaccaataATAACTTCGTATAGCATACATTATACGAAGTTATACC	to amplify loxP-RFP-loxP
JB632_CG32-42_RH_loxP_F	acgaagttatTATTGGTGACTAAAGCTATTTAAGTG	to amplify RHA
JB633_CG32-42_RH_XhoI_R	actcgattgacggaagagccCTTCAGGGGATCAAGGAAC	to amplify RHA
JB265_Gibson_pEntr_1F	AAGGGTGGGCGCGCCGAC	to amplify pEntr backbone
JB266_Gibson_pEntr_1R	GGTGAAGGGGCGGCCGC	to amplify pEntr backbone
JB517_CG32736_pEntr_F	ccgcggccgccccccttcaccATGAGTCCGTACAGCGGATC	to construct pEntr_sloth1
JB518_CG32736_pEntr_R	gggtcggcgcgcccaccctTTAGTTGGTGTTATTCGCGG	to construct pEntr_sloth1
JB519_CG32736_nostop_pEntr_R	gggtcggcgcgcccaccctTGTTGGTGTTATTCGCGGCT	to construct pEntr_sloth1
JB404_CG42308_pEntr_F	ccgcggccgccccccttcaccATGCCCGCCGGAGTTTCC	to construct pEntr_sloth2
JB405_CG42308_pEntr_R	gggtcggcgcgcccaccctTTATGCAGATTCCGGTGGC	to construct pEntr_sloth2
JB509_CG42308_nostop_pEntr_R	gggtcggcgcgcccaccctTGCAGATTCCGGTGGCTT	to construct pEntr_sloth2
JB742_hSMIM4_gBlock (incorrect reverse seq)	ccgcggccgccccccttcaccATGTTTACAAGGGCACAAGTTCGCCGGATACTGCAACGAGTACCAGGTAAACAGCGCTTTGGCATCTATCGCTTCCTGCCATTCTTTTTTGTACTCGGCGGTACTATGGAGTGGATAATGATTAAAGTTCGAGTGGGCCAGGAGACATTCTACGATGTCTATAGGCGAAAAGCTAGTGAACGCCAGTATCAAAGGCGATTGGAAGACGAGgggtcggcgcgcccaccctt	to construct pEntr_hSMIM4
JB732_hSMIM4_pEntr_F	ccgcggccgccccccttcaccATGTTTACAAGGGCACAAGTTC	to construct pEntr_hSMIM4
JB733_hSMIM4_stop_pEntr_R	gggtcggcgcgcccaccctttctattaCTCGTCTTCCAATCGCCTT	to construct pEntr_hSMIM4
JB743_hSMIM4_nostop_pEntr_R	gggtcggcgcgcccaccctTCTCGTCTTCCAATCGCCTT	to construct pEntr_hSMIM4
JB526_hC12orf73_gBlock	CCGCGGCCGCCCCCTTcaccATGCCCGCGGGCGTGCCCATGTCCACCTACCTGAAAATGTTCGCAGCCAGTCTCCTGGCCATGTGCGCAGGGGCAGAAGTGGTGCACAGGTACTACCGACCGGACCTGACAATACCTGAAATTCCACCAAAGCGTGGAGAACTCAAAACGGAGCTTTTGGGACTGAAAGAAAGAAAACACAAACCTCAAGTTTCTCAACAGGAGGAACTTAAATAAAAGGGTGGGCGCGCCGACCC	to construct pEntr_hC12orf73
JB548_entr_c12orf73_nostop_R	gcccacccttTTTAAGTTCCTCCTGTTGAG	to construct pEntr_hC12orf73
JB549_entr_c12orf73_nostop_F	ggaacttaaaAAGGGTGGGCGCGCCGAC	to construct pEntr_hC12orf73
JB725_CG3242_genomic_pEntr_F	ccgcggccgccccccttcaccTCATTAGCGATGACAGCG	to construct pEntr_sloth1-sloth2 genomic
JB726_CG3242_genomic_pEntr_R	gggtcggcgcgcccaccctTAAACGTGGCGTCTTTTGAATG	to construct pEntr_sloth1-sloth2 genomic
JB727_CG3242_transcript_pEntr_F	ccgcggccgccccccttcaccAATCGAACAGCTGATTGCTG	to construct pEntr_sloth1-sloth2 transcript
JB728_CG3242_transcript_pEntr_R	gggtcggcgcgcccaccctTCTTAAATAGCTTTAGTCACCAATAACTTG	to construct pEntr_sloth1-sloth2 transcript
JB761_pEntr_genomicCG32_CG42del_F	actaagcaaaCACTGTGTACTAGACAAGTTATTGGTG	to construct pEntr_sloth1-sloth2 genomic derivatives
JB762_pEntr_genomicCG32_CG42del_R	gtacacagtgTTTGCTTAGTTGGTGTTATTCG	to construct pEntr_sloth1-sloth2 genomic derivatives
JB763_pEntr_genomicCG32del_CG42_F	ctgaaaacacGCAAAATGCCCGCCGGAG	to construct pEntr_sloth1-sloth2 genomic derivatives
JB764_pEntr_genomicCG32del_CG42_R	ggcattttgcGTGTTTTCAGCCGGCGGTTATATAATTC	to construct pEntr_sloth1-sloth2 genomic derivatives
JB510_sfGFP_Wal10-roe-XbaI_F	agtggtgattcgagggtaccTCggaggctccggtgtgtc	to construct pWalium10-roe-sfGFP
JB511_sfGFP_Wal10-roe-XbaI_R	gcagatcagaactagtttgcctacttgtacagctcatccatgc	to construct pWalium10-roe-sfGFP
JB533_PD43265F	GAAAGAAGCGCTTCGGTGTC	qPCR primers for sloth1
JB534_PD43265R	TCCACGTAGTTCTTCGCCTG	qPCR primers for sloth1
JB540_PD43573F	AGGACTTGCGCGTCTACATC	qPCR primers for sloth2
JB539_PD43573R	GATCCACCTGTGTGCTGTGT	qPCR primers for sloth2
JB713_Rp49_F	ATCGGTTACGGATCGAACAA	qPCR primers for Rp49
JB714_Rp49_R	GACAATCTCCTTGCGCTTCT	qPCR primers for Rp49
JB717_Gapdh_F	CCAATGTCTCCGTTGTGGA	qPCR primers for Gapdh
JB718_Gapdh_R	TCGGTGTAGCCCAGGATT	qPCR primers for Gapdh
JB1110_CG32736_indel_1F	CCTTAAAATTGGCGAAACCA	PCR primers to genotype and sequence sloth1-KO fly lines and S2R+ cell lines
JB1111_CG32736_indel_1R	TAAAAAGAAGAGCGGCAGGA	PCR primers to genotype and sequence sloth1-KO fly lines and S2R+ cell lines
JB1114_CG42308_indel_1F	CGCGAATAACACCAACTAAGC	PCR primers to genotype and sequence sloth2-KO fly lines and S2R+ cell lines
JB1115_CG42308_indel_1R	ATGTAGACGCGCAAGTCCTC	PCR primers to genotype and sequence sloth2-KO fly lines and S2R+ cell lines
JB580_CG32736_CG42308_geno_1F	gagcagtcgccgaaatagtc	PCR primers to genotype and sequence dKO fly lines and S2R+ cell lines
JB587_CG32736_CG42308_geno_4R	tgaaacctttccctgtcac	PCR primers to genotype and sequence dKO fly lines and S2R+ cell lines
JB787_CG3242_LHA_F	tcgaaaagttgtgcctgatg	PCR primers to genotype Gal4-KI flies (left homology region)
JB662_Gal4seq1R	agcggagacctttttggtttt	PCR primers to genotype Gal4-KI flies (left homology region)
JB659_3P3dsred_seq1F	ACTCCAAGCTGGACATCACC	PCR primers to genotype Gal4-KI flies (right homology region)
JB790_CG3242_RHA_R	cgatgagccggctataaaaa	PCR primers to genotype Gal4-KI flies (right homology region)

Supplemental File 3

pEntr plasmid	Expression plasmid	Final plasmid name	Alternative name	Fly Insertion site
pEntr_sloth1_stop	pWalium10-roe	pWalium10-sloth1	UAS-sloth1	attP2
pEntr_sloth2_stop	pWalium10-roe	pWalium10-sloth2	UAS-sloth2	attP2
pEntr_sloth2_stop	pValium10-roe	pValium10-sloth2	UAS-sloth2	attP40
pEntr_hSMIM4_stop	pWalium10-roe	pWalium10-hSMIM4	UAS-hSMIM4	attP2
pEntr_hC12orf73_stop	pWalium10-roe	pWalium10-hC12orf73	UAS-hC12orf73	attP2
pEntr_sloth1-sloth2 transcript	pWalium10-roe	pWalium10-sloth1-sloth2 transcript	UAS-sloth1-sloth2	attP2
pEntr_sloth1-sloth2 genomic	pBID-G	pBID-{sloth1-sloth2}	{sloth1-sloth2}	attP40
pEntr_Δsloth1-sloth2 genomic	pBID-G	pBID-{Δsloth1-sloth2}	{Δsloth1-sloth2}	attP40
pEntr_sloth1-Δsloth2 genomic	pBID-G	pBID-{sloth1-Δsloth2}	{sloth1-Δsloth2}	attP40
pEntr_sloth1_nostop	pWalium10-roe-sfGFP	pWalium10-sloth1-sfGFP	UAS-sloth1-sfGFP	
pEntr_sloth1Δmito_nostop	pWalium10-roe-sfGFP	pWalium10-sloth1Δmito-sfGFP	UAS-sloth1Δmito-sfGFP	
pEntr_sloth1mitoonly_nostop	pWalium10-roe-sfGFP	pWalium10-sloth1mitoonly-sfGFP	UAS-sloth1mitoonly-sfGFP	
pEntr_sloth2_nostop	pWalium10-roe-sfGFP	pWalium10-sloth2-sfGFP	UAS-sloth2-sfGFP	
pEntr_sloth2Δsec_nostop	pWalium10-roe-sfGFP	pWalium10-sloth2Δsec-sfGFP	UAS-sloth2Δsec-sfGFP	
pEntr_sloth2onlysec_nostop	pWalium10-roe-sfGFP	pWalium10-sloth2seconly-sfGFP	UAS-sloth2seconly-sfGFP	
pEntr_Tim8_nostop	pAWH	Act-Tim8-HA		
pEntr_Tim13_nostop	pAWH	Act-Tim13-HA		
pEntr_BFP_nostop	pAWH	Act-BFP-HA		
pEntr_sloth1_nostop	pAWH	Act-sloth1-HA		
pEntr_sloth2_nostop	pAWH	Act-sloth2-HA		
pEntr_BFP_nostop	pAWF	Act-BFP-FLAG		
pEntr_sloth1_nostop	pAWF	Act-sloth1-FLAG		
pEntr_sloth2_nostop	pAWF	Act-sloth2-FLAG		
pEntr_BFP_nostop	pMK33-GW-SBP	pMK33-BFP-SBP	MT-BFP-SBP	
pEntr_sloth1_nostop	pMK33-GW-SBP	pMK33-sloth1-SBP	MT-sloth1-SBP	
pEntr_sloth2_nostop	pMK33-GW-SBP	pMK33-sloth2-SBP	MT-sloth2-SBP	
pEntr_sloth1_stop	pMK33-GW	pMK33-sloth1	MT-sloth1	
pEntr_sloth2_stop	pMK33-GW	pMK33-sloth2	MT-sloth2	